POLITECNICO
MILANO 1863

SCUOLA DI INGEGNERIA INDUSTRIALE
E DELL'INFORMAZIONE

Detection of Perampanel in saliva by SERS using substrates produced by PLD

Masters of Science in
Materials Engineering and Nanotechnologies

Author: **Luca Stefani**

Student ID: 944849
Advisor: Prof. Paolo Maria Ossi
Co-advisors: Prof. Matteo Tommasini, Prof. Andrea Lucotti, Dr. Sebastiano Trusso
Academic Year: 2021-2022

Ma, per essere uno scienziato che apre nuove vie, alla sua intelligenza mancava il dono del fortuito, la forza che, con scoperte impreviste viola la sterile armonia del prevedibile. Nello stesso modo, per operare il bene, alla sua coerenza di principi mancava l'incoerenza del cuore, che non conosce casi generali, ma solo il particolare, ed è grande perché agisce nella sfera del piccolo.

— **Borìs Pasternak** Il dottor Živago

Acknowledgements

Sono finalmete giunto alla fine di questo lungo cammino. Guardandomi in dietro mi rendo conto della fortuna che ho avuto avere così tante persone che mi hanno dato così tanto. Per questo voglio ringraziarle per tutte le volte che mi hanno aiutato ed incoraggiato in questi anni. Ognuno ha contribuito in qualche modo alla mia crescita, con un gesto, con una parola o semplicemte con la sua presenza. Ho ricevuto tantissimo e a volte mi chiedo se sarò mai in grado di restituire anche solo una minima parte di tutto quello che ho ricevuto. Devo provarci. Questi ringrazimenti possono essere buon inizio. Dedico questa tesi a tutti voi che mi avete aiutato, confortato, accompagnato ed incoraggiato!

À ma maman, la persona ai cui devo di più di tutti, grazie per avermi sempre spronato ed incoraggiato ad essere sempre la versione migliore di me stesso. *Merci pour tout.*
Al mio babbo per esserci sempre stato nei momenti più importanti, per avermi insegnato cosa vuol dire farsi un mazzo tanto, per avermi sempre protetto e capito.
A Matte e Gio, i miei fratellini, non sono sempre stato un bravo fratello maggiore, ma so che nonostante tutto mi volete bene.
Al nonno ed alla nonna per tutto l'amore che mi avete dato, sempre e comunque.
A Tommy per essere il mio fratellone, per tutte le botte che ci siamo dati e che ci daremo ancora, per avermi sempre aiutato e sopportato.
A Leo, ad Anto, a Pietro i miei cugini, i miei migliori amici.
A tutta la famiglia Stefani.
A Tommy che mi sopporta dal liceo e mi è stato accanto in questi cinque anni.
A Tommy Maio.
A Ivana per tutte le discussioni che abbiamo avuto e per tutto quello che mi ha insegnato.
Ad Aurora.
A Sam.
Ad Arman, Davide, Daniele.
A Irene, Alessia, Paola, Shamir.
A Marco, a Pier, a Laura.
A Gabriela.

Abstract

In my thesis, I used substrates decorated with gold nanoparticles deposited via Pulsed Laser Deposition (PLD) as SERS sensors for Therapeutic Drug Monitoring (TDM) of an anti-epileptic drug such as Perampanel (PER).

In the first part of my thesis, I demonstrated that it is possible to detect dilute PER in saliva through SERS analysis and that it is possible to treat the sample in a way that optimizes the SERS response through manipulation of the pH of the salivary solution. Next, I determined the qualitative response of the SERS sensors with respect to varying concentrations of PER by plotting calibration curves against the intensity PER markers which showed that the SERS signal intensity of the PER present in saliva is linearly proportional to the concentration of the drug in the solution.

In the second part of the thesis, I investigated the possibility of pre-treatment of diluted PER solutions in saliva in order to obtain samples that allow better identification of PER through SERS. I have shown that using a phase separation process it is possible to extract all the diluted PER in saliva, from the saliva phase to the chloroform phase. Finally, it was shown that by properly treating the PER extract solubilized in chloroform it is possible to regain a solution of PER diluted in methanol. PER can be detected in the SERS signal demonstrating that the entire phase separation process is a viable route to obtaining more accurate SERS measurements.

Solution treatment through phase separation opens the door to the possibility of approaching PER detection in solutions at low concentrations. Since as demonstrated in this thesis, through evaporation of the diluted PER solution in chloroform, it is possible, to re-concentrate the PER and so as to obtain solutions in methanol with higher PER concentrations than the starting chloroform solutions.

Abstract in lingua italiana

Nella mia tesi ho utilizzato dei substrati decorati con nanoparticelle d'oro depositate tramite Pulsed Laser Deposition (PLD) come sensori SERS per il Therapeutic Drug Monitoring (TDM) di un farmaco anti-epilettico come il Perampanel (PER).

Nella prima parte della mia tesi ho dimostrato che è possibile individuare il PER di diluito nella saliva attraverso l'analisi SERS e che è possibile trattare il campione in modo da ottimizzare la risposta SERS attraverso la manipolazione del pH della soluzione salivare. In seguito ho determinato la risposta qualitativa dei sensori SERS rispetto a concentrazioni variabili di PER tracciando delle curve di calibrazione rispetto ai marker del PER che hanno mostrato che l'intensità del segnale SERS del PER presente nella saliva è linearmente proporzionale alla concentrazione del farmaco in soluzione.

Nella seconda parte della tesi ho studiato la possibilità di pre-trattamento delle soluzioni di PER diluito in saliva in modo da ottenere dei campioni che permettono una migliore identificazione del PER attraverso SERS. Ho dimostrato che usando un processo di separazione di fase è possibile estrarre tutto il PER diluito nella saliva, dalla fase saliva alla fase cloroformio. Infine, è stato dimostrato che trattando adeguatamente l'estratto di PER solubilizzato nel cloroformio è possibile riottenere una soluzione di PER diluito in metanolo. Nel segnale SERS è possibile individuare il PER a dimostrazione che l'intero processo di separazione di fase rappresenta una strada percorribile per l'ottenimento di misure SERS più accurate.

Il trattamento della soluzione attraverso la separazione di fase apre le porte alla possibilità di avvicinarsi all'individuazione del PER in soluzioni a basse concentrazioni. Poiché come dimostrato in questa tesi, attraverso l'evaporazione della soluzione di PER diluito in cloroformio, è possibile, riconcentrare il PER e in modo da ottenere delle soluzioni in metanolo con concentrazioni di PER più elevate di quelle delle soluzioni di cloroformio di partenza.

Contents

List of Figures

List of Tables

1 | Introduction

Epilepsy is the most common known neurological disorder, affecting between 0.6% and 1% of the world's population [24]. An estimated 2.4 million new cases are diagnosed each year, mostly in low- and middle-income countries. Epilepsy consists of a chronic disorder of the brain that manifests as recurrent seizures. These are episodes of muscle spasm, involving the entire body. These seizures can also cause loss of consciousness and loss of control of some functions of the body. The frequency of seizures varies widely, from a few times a year to several per day. Perampanel (PER) is a newly developed Anti-epileptic Drug (AED). PER was approved in 2012 and its efficacy and safety have been investigated since then. AEDs fall under the category of drugs with a *Narrow Terapeutic Index* (NTI). This means that the dose range in which the drug is effective without causing side effects is very narrow. Patients who have received a dose that exceeds the upper limit of this range will experience side effects, while for patients who have received a dose below the lower limit of this range, seizures will not be controlled.

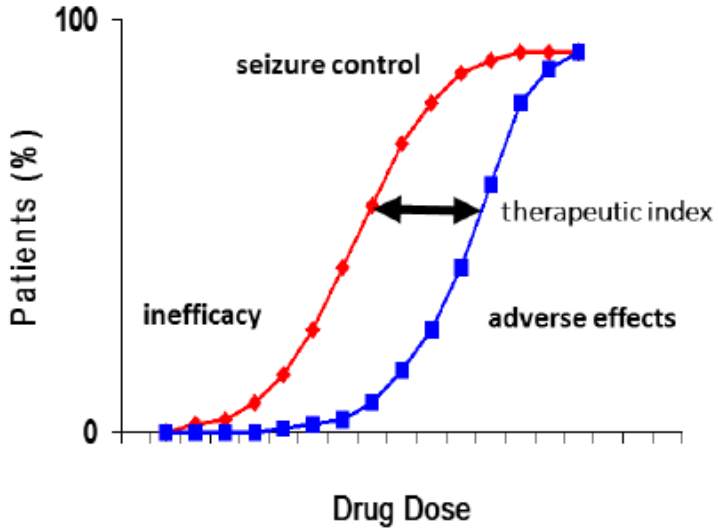

Figure 1.1: Antiepileptic drug therapeutic index. The red curve indicates the minimum effective drug dose, while the blue the limiting dosage curve to avoid toxic effects [22].

To avoid these problems, it is necessary to provide a tailored treatment that requires careful fine-tuning of the drug dosage for each specific patient, since the range of the therapeutic index varies from person to person [11]. A technique called *Therapeutic Drug Monitoring* (TDM) is commonly employed for this purpose. TDM involves constantly measuring the concentration of the drug in the patient's biological fluids, such as plasma [14]. High performance liquid chromatography (HPLC) coupled with mass spectroscopy (MS) is the most widely used laboratory technique for TDM. These measurements are very accurate and reliable, but are time consuming and expensive. A common test can take 1 to 4 days to perform and the cost of a single analysis is kept between €15 and €30 [22]. This limits the population of patients who can benefit and the frequency with which testing can be performed on a patient. Therefore, research is focusing on developing alternative techniques that can speed up the process. Surface Enhanced Raman Spectroscopy (SERS), is certainly among the most promising. SERS allows the detection of molecules present even at very low concentrations. By exploiting nanostructured metal surfaces, it is possible to obtain an increase in the response signal when the surface is irradiated with a laser. If the analyte molecule has been adsorbed on the surface, its Raman signatures will be increased in intensity through the process of plasmonic enhancement, thus allowing their detection. Among the biological fluids of interest for TDM of AED is emerging interest in saliva that begins to be increasingly used given the potential advantages it has over serum or blood especially from the point of view of the collection. In fact, the sampling of saliva is much easier since the presence of a highly skilled operator is not required and the stress on the patient is minimized [20], in addition, the concentration of drug in saliva generally reflects the amount of pharmacologically active in blood that has not bound to proteins in the serum.

The objective of this thesis is to identify through SERS measurements the PER present in the patient's saliva. Through the use of SERS substrates decorated with gold nanoparticles produced by Pulsed Laser Deposition (PLD) I will try to define the most suitable chemical and physical conditions for the SERS detection of PER solubilized in saliva. Finally, the qualitative response of SERS sensors produced via PLD with respect to varying concentrations of PER will be determined.

The research conducted in this thesis work has shown the possibility of detecting the PER solubilized in saliva through SERS measurements made on substrates produced via PLD. Furthermore, it has been shown that the signal of PER, measured through SERS spectroscopy, is directly proportional to its concentration in the salivary solution. Finally, it was shown that the salivary solution containing PER can be treated by a phase separation process, using chloroform, in order to obtain samples that allow a better

identification of PER by SERS spectroscopy.

2 | Methods

2.1. Raman spectroscopy

Raman spectroscopy (RS) is a technique based on the inelastic scattering of radiation by a sample which can be solid, liquid or a gas. Through their characteristic spectrum it provides information on chemical and physical structures of the analysed substances [6]. It is named after Sir C.V. Raman who first observed the physical phenomenon: when a monochromatic light is scattered from a sample, most of the radiation is scattered at constant energy and frequency which is due to elastic (Rayleigh) scattering, but a small fraction of light with different energy is also observed. The energy of the incoming photon gets modified by inelastic interaction with the quantum vibrational states of the sample. The difference in energy due to this inelastic processes, typically reported in wavenumbers (i.e., cm^{-1}), is known as the Raman shift and is the key factor in Raman spectroscopy. The exchanged energy strongly depends on the position of vibrational levels, which in turn is determined by the molecular structure of the system. As a result, a Raman spectrum results in an unique fingerprint of a molecule.

2.1.1. Classical theory of Raman scattering

In this section, the Raman scattering will be explained using a classical treatment. Both the sample and the electromagnetic radiation will be described in a classical way. The assumption is that the incident radiation is a monochromatic plane wave and is expressed in terms of an electric field vector $\boldsymbol{E}$ harmonically oscillating at the frequency ω_L:

$$\mathbf{E} = \mathbf{E}_0 \cos(\omega_L t) \tag{2.1}$$

The incoming light induces a polarization in the sample and the corresponding frequency dependent induced electric dipole $\boldsymbol{p}$, in the linear approximation, is proportional to the incident electric field through the polarizability tensor:

$$\mathbf{p} = \alpha \cdot \mathbf{E} \tag{2.2}$$

The polarizability tensor is an intrinsic property of the molecule and depends on the nuclear coordinates of atoms. As a result, the polarizability changes if atoms move from their equilibrium positions because of molecular vibrations. Considering one single molecule which can vibrate freely, the dependence of the polarizability on all the normal coordinates of the molecule can be expressed as a Taylor series:

$$\alpha = \alpha_0 + \sum_k \left(\frac{\partial \alpha}{\partial Q_k}\right)_0 Q_k + ... \tag{2.3}$$

where the index 0 stands for the equilibrium configuration. Using the linear approximation we neglect the higher order terms are neglected.[15] The summation in equation 2.3 includes all the normal modes of the molecule, i.e. $3N - 6$, where N is the number of atoms in a non-linear molecule [6].

In the harmonic approximation, the variation of the k^{th} normal coordinate in time is expressed by a simple cosine function oscillating at the characteristic frequency ω_k:

$$Q_k = Q_{k_0} \cos(\omega_k t + \delta_k) \tag{2.4}$$

Considering, for simplicity, one normal mode only and substituting equation 2.4 into equation 2.3, the polarizability tensor as a function of the k^{th} vibration is obtained:

$$\alpha = \alpha_0 + \left(\frac{\partial \alpha}{\partial Q_k}\right)_0 Q_{k_0} \cos(\omega_k t + \delta_k) \tag{2.5}$$

The final expression of the induced electric dipole is derived introducing equations 2.1 and 2.5 into 2.2:

$$\mathbf{p} = \alpha_0 \mathbf{E}_0 \cos(\omega_L t) + \left(\frac{\partial \alpha}{\partial Q_k}\right)_0 \mathbf{E}_0 Q_{k_0} \cos(\omega_k t + \delta_k) \cos(\omega_L t) \tag{2.6}$$

Equation 2.6 can be manipulated using Werner's trigonometric formulas and rewritten in a more compact form:

$$\mathbf{p} = \alpha_0 \mathbf{E}_0 \cos(\omega_L t) + \frac{1}{2}\left(\frac{\partial \alpha}{\partial Q_k}\right)_0 \mathbf{E}_0 Q_{k_0} [\cos((\omega_L - \omega_k)t - \delta_k) + \cos((\omega_L + \omega_k)t + \delta_k)] \tag{2.7}$$

The induced electric dipole moment in equation 2.7 contains cosine functions oscillating at three different frequencies, which are the result of three distinct scattering processes occurring during light-matter interaction:

- The first term, proportional to the equilibrium polarizability tensor and oscillating at the frequency of the incoming radiation ω_L, is the Rayleigh component and corresponds to elastic scattering. This is by far the most probable scattering event. No energy is exchanged with the molecule and the energy of the incident radiation is the same as the energy of the scattered one.
- The second term, proportional to the derived polarizability tensor, is the Raman component and arises because of inelastic processes. Some energy is exchanged with the sample and the frequency of the scattered radiation is modified by the frequency of the considered normal mode of vibration. When the incident radiation gives energy to the molecule, the outgoing radiation is redshifted and oscillates at frequency $\omega_L - \omega_k$ (Stokes component); on the other hand, when the incident radiation acquires energy from the molecule, the outgoing radiation is blue-shifted and oscillates at frequency $\omega_L + \omega_k$ (anti-Stokes component).

Equation 2.7 underlines a particular feature of Raman spectroscopy: changing the excitation source, that means a change of ω_L, There is no change in Raman spectra. Indeed the position of the peaks depends only on the vibrational frequency ω, so using another excitation line leads to a shift of the whole spectrum. Another important information from equation 2.7 is that only vibrations that change the polarizability yield Raman scattering. This mean that the quantity $\left(\frac{\partial \alpha}{\partial Q}\right)$, must be different from zero if Raman signal is to be observed. This is the so-called Raman selection rule.

2.1.2. Limits of classic description

The classical approach fails to describe completely the Raman scattering . It correctly predicts that Raman scattering should be weaker than Rayleigh scattering, and that polarization and scattering intensity, are linear with respect to the exciting laser intensity. But, according to classical theory, the relative Stokes/anti-Stokes ratio is predicted to be:

$$\frac{I_S}{I_{aS}} \propto \frac{(\omega_L - \omega)^4}{(\omega_L + \omega)^4} = \frac{{\omega_S}^4}{{\omega_{aS}}^4} < 1 \tag{2.8}$$

this mean that Stokes intensities should be lower than anti-Stokes intensities. This is in contrast with experimental data, because anti-Stokes lines are always less intense than Stokes lines. Boltzmann distribution is the major factor in determining relative Stokes and anti-Stokes intensity. The excited vibrational state will be only the thermally populated one, so Stokes intensity will be much larger than anti-Stokes.

As a result, even if the classical theory correctly predicts the position of Raman lines,

it fails to describe the exact intensity ratio. To better understand the point a quantum approach of the phenomenon is needed.

2.1.3. Quantum description

The classical approach can be improved using quantum mechanics. Actually, only the molecule (or the crystal) is treated quantum mechanically, while the electromagnetic field is still treated in classical way according to Maxwell's equations. This kind of approach is called semi-classical [1].

The potential energy for a diatomic molecule can be described by the Morse potential, which can be further simplified through the harmonic approximation. This quantum oscillator has quantized energy level, meaning that the energy eigenvalues are discrete and labelled by a quantum number $n = 0, 1, 2, ...$ Solving the Schroedinger's equation using the harmonic approximated potential, an expression for the eigenvalues is found:

$$E_n = \hbar\omega\left(n + \frac{1}{2}\right) \tag{2.9}$$

Now it's worth to introduce what virtual states are. They are transition states that do not correspond to an eigenstate of the system. That makes them very unstable levels. So, if the photon energy is not enough to promote the electron to a real state of the system, it goes to a virtual state and then rapidly decay to a proper lower level of the system.

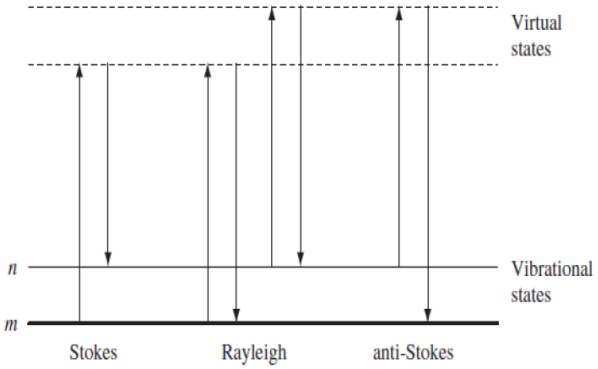

Figure 2.1: Scheme of scattering processes in Raman spectroscopy.

The relative position of the initial and final states indicate the scattering type, whether elastic or inelastic and if it Stokes or anti-Stokes (as can be seen in Figure 2.1). Due to Boltzmann population distribution, the anti-Stokes scattering will be less probable than the Stokes, because the starting energy level is higher energy. So, by considering

Boltzmann distribution, n, expressed as:

$$n(\omega, T) = \frac{1}{e^{\frac{\hbar\omega}{kT}} - 1} \tag{2.10}$$

The relative ratio Stokes/anti-Stokes becomes:

$$\frac{I_S}{I_{aS}} \propto \frac{(\omega_L - \omega)^4}{(\omega_L + \omega)^4} \exp\left(\frac{\hbar\omega}{k_b T}\right) \tag{2.11}$$

The ratio in equation 2.11 is larger than 1 thanks to the presence of the exponential factor. This is in accord with experiments. Moreover, the ratio decreases with increasing temperature: the intensity of the anti-Stokes peak depends on the occupancy of the initial state and the population of excited vibrational levels grows as the temperature increases.

2.2. Surface Enhanced Raman Scattering (SERS)

There are two intrinsic limitations that reduce the applicability of conventional Raman spectroscopy when high sensitivity is required. When there is a weak signal and a strong fluorescence emission. The first drawback is related to the inherently small probability of the Raman process to occur. The cross-section of the Raman event is 12 to 14 orders of magnitude lower than the fluorescence one [13]. Indeed, only one in every 10^7 photons is inelastically scattered, while the large majority of photons undergo elastic scattering [26]. The second disadvantage is represented by strong fluorescence emission, especially when visible exciting radiation is used, which can prevent the detection of the Raman signal.

To overcome those issues, a huge intensifcation of Raman signals coming from molecules can be achieved when the analyte is close to the surface of a substarte decorated with metallic nanostructure. This is the principle of Surface Enhanced Raman Scattering (SERS), that has gradually become a valuable technique able to combine the spectroscopic fingerprint typical of RS with a very large sensitivity as requested by trace detection in chemical, biological, medical, forensic, and food sciences. J.A. Creighton, provided a first explanation about the origin of the enhancement: the amplification of the signal was not caused by an increase in the surface area, as supposed by Fleischmann, but because of strong electric fields at the metal surface (according to Jeanmarie and Van Duyne) or due to the formation of a molecule-metal complex (according to Albrecht and Creighton). An important review was published in 1985 by M. Moskovits, who related the intensification effect with the excitation of collective oscillations of conduction electrons in the metal nanostructure. In the following years, the technological improvement in Raman in-

strumentation, the advancement of nanotechnology and the possibility of single-molecule detection have fostered the development of SERS as a powerful tool for analytical investigations, although some theoretical aspects regarding the exact enhancement mechanism are not fully clarified yet [6, 21].

2.2.1. Optical properties of materials

To better understand the SERS working principle, concepts as plasmonic effect and its resulting properties have to be introduced. A first approach concerning the interaction between electromagnetic radiation and a metal is given by the Drude model. The metal is assumed to consist of fixed, positively charged ions surrounded by free to-move electrons. The considered relevant collisions electrons can undergo are with ions. After a collision the electron velocity depends only on the local temperature distribution and it is independent from the velocity before the collision [17]. Let's consider the motion of an electron, of charge (-e), under the action of an external electric field $\boldsymbol{E}$:

$$\frac{dp}{dt} = -\frac{p}{\tau} - e\mathbf{E} \tag{2.12}$$

where p is the momentum and τ is a charatcteristic collision time.

More precisely τ is the relaxation time, which is of the order of 10^{-14} seconds at room temperature. In general, the reciprocal of the relaxation time is defined, which is the damping term $\gamma = \frac{1}{\tau}$, that takes into account the damping due to collisions. Considering a time depended electric field $\mathbf{E} = \mathbf{E}_0 e^{-i\omega t}$, eq. 2.12 becomes:

$$m\frac{d^2x}{dt^2} + \gamma m\frac{dx}{dt} = -e\mathbf{E} \tag{2.13}$$

The solution of equation 2.13 is:

$$x(t) = \frac{e}{m(\omega^2 + i\gamma\omega)}\mathbf{E}(t) \tag{2.14}$$

The displaced electrons contribute to the macroscopic polarization of the metal. This is clear by considering the electron dipole moment $\mu = -ex$. By substituting in eq. 2.14 the polarization $P = n\mu$, with n indicating the electron density:

$$P = n\mu = -\frac{ne^2}{m(\omega^2 + i\gamma\omega)}\mathbf{E}(t) \tag{2.15}$$

Remembering that the electric displacement is $D = \varepsilon_0\mathbf{E} + P$ and that for linear, isotropic

and non-magnetic media $D = \varepsilon_0 \varepsilon E$, it is possible to obtain:

$$\varepsilon(\omega) = 1 + \frac{P}{\varepsilon_0 \mathbf{E}} = 1 - \frac{\omega_p}{(\omega^2 + i\gamma\omega)} \tag{2.16}$$

where $\omega_p = \sqrt{\frac{ne^2}{\varepsilon_0 m}}$ is the plasma frequency.

The dielectric function $\varepsilon(\omega, k)$ depends both on the frequency and on the wavevector of the electromagnetic radiation. Yet, considering wavelengths in the UV-visible range those are significantly longer than all characteristic material dimensions, such as the size of the unit cell or the electron mean free path, so the dependence on the wavevector can be neglected. Furthermore, in general $\varepsilon(\omega)$ is a complex number made by a real and imaginary part:$\varepsilon(\omega) = \varepsilon_1(\omega) + i\varepsilon_2(\omega)$. Thus, explicitly expressing the dielectric function terms, we have:

$$\varepsilon_1(\omega) = Re\{\varepsilon(\omega)\} = 1 - \frac{{\omega_p}^2}{\omega^2 + \gamma^2} \tag{2.17}$$

$$\varepsilon_2(\omega) = Im\{\varepsilon(\omega)\} = \frac{{\omega_p}^2 \gamma}{\omega(\omega^2 + \gamma^2)} \tag{2.18}$$

For large frequencies, $\omega >> \gamma$ the damping term can be neglect so eqns. 2.17 and 2.18 reduce to:

$$\varepsilon_1(\omega) = 1 - \frac{{\omega_p}^2}{\omega^2} \tag{2.19}$$

$$\varepsilon_2(\omega) = \frac{{\omega_p}^2 \gamma}{\omega^3} \tag{2.20}$$

Three different situations can be considered according to eqns. 2.19 and 2.20:

- When $\omega < \omega_p$, $\varepsilon < 0$, the refractive index ($\mathrm{n} = \sqrt{\varepsilon(\omega)}$) is purely imaginary,and the reflectance is equal to 1. The incident radiation is completely reflected back and cannot propagate in the material, where an evanescent wave decays exponentially in the

  first tens of nanometers below the surface (metallic domain).

- When $\omega > \omega_p$, $\varepsilon > 0$, the refractive index is real and light is transmitted through the metal (transparency domain).

- When $\omega = \omega_p$, $\varepsilon = 0$, a collective in-phase longitudinal oscillations of free conduction electrons are observed. The quanta of this oscillation are called bulk plasmons, each corresponding to an energy equal to $\hbar\omega_p$.

This model is an oversimplification and real metals exhibit large discrepancies. First of all, the imaginary part of the dielectric constant has been neglected; secondly, bound

electrons, responsible for interband transition (especially in transition metals with inner d bands), have not been considered; and thirdly, the polarization background of ions has not been included in the model.

Plasmons can be found both in the bulk or on the surface of metals. In particular, the last ones are of high interest for SERS. Surface plasmons, which are confined to surfaces, can occur only at interface between the metal and a dielectric material. In general, they can be present at the interface between a material with positive $\varepsilon_1(\omega)$, like a dielectric, and a material characterized by negative $\varepsilon_1(\omega)$ at the given frequency of light, like a metal. So, the two materials need to have opposite sign of the real part of their dielectric permittivity. The condition is not sufficient since the magnitude of the real part of the permittivity in the negative permittivity region should be larger than the magnitude of the permittivity in the positive permittivity region to have the light confinement on the surface. Surface plasmons are characterized by the frequency:

$$\omega_{SP} = \frac{\omega_p}{\sqrt{1 - \varepsilon_{dielectric}}}$$

2.2.2. Electromagnetic enhancement

Localized surface plasmons are another fundamental collective excitation of electrons. If surface plasmons are dispersive waves coupled to the electron plasma of a conductor at the interface with a dielectric, the localized surface plasmon are non-propagating excitations of the conduction electrons of metallic nanostructure coupled to electromagnetic field. So, it is the result of the confinement of surface plasmons in a nanoparticle with a size lower than the excitation light wavelength. Due to the presence of an external electric field ($\mathbf{E}_0$), the electronic cloud of a nanoparticle oscillates generating a dipole, which in turns generates a local electric field. The total electric field is now:

$$\mathbf{E}_{TOT} = \mathbf{E}_0 + \mathbf{E}_{SP} \tag{2.21}$$

In a quasi-static approximation one considers the nanoparticles as homogeneous and isotropic spheres embedded in an isotropic medium. It means that the size of the nanoparticles is much lower than the excitation light, in such a way the external electric field can be assumed to be static. By solving the Laplace equation, it is possible to evaluate the external and internal potential, which induces a dipole moment on the sphere equal to:

$$p = 4\pi\varepsilon_0\varepsilon_m a^3 \frac{\varepsilon - \varepsilon_m}{\varepsilon + 2\varepsilon_m}\mathbf{E}_0 \tag{2.22}$$

where ε_m is the dielectric of the medium outside the nanoparticle, α the radius of the nanoparticle and ε is the dielectric of the metal. The polarizability can now be introduced, since $p = \varepsilon_0 \varepsilon_m \alpha \mathbf{E}_0$, as follows:

$$\alpha = 4\pi a^3 \frac{\varepsilon - \varepsilon_m}{\varepsilon + 2\varepsilon_m} \tag{2.23}$$

The induced electric field can also be calculated, which yields:

$$\mathbf{E}_{IN} = \frac{3\varepsilon_m}{\varepsilon + 2\varepsilon_m} \mathbf{E}_0 \tag{2.24}$$

Both the equations 2.23 and 2.24 may reach a resonant enhancement when $|\varepsilon + 2\varepsilon_m|$ reaches a minimum. Neglecting the imaginary term of the dielectric constant, so considering just $\varepsilon_1(\omega) = Re\{\varepsilon(\omega)\}$, the resonance condition becomes:

$$\varepsilon_1(\omega) = 1 - \frac{{\omega_p}^2}{\omega^2} = -2\varepsilon_m \tag{2.25}$$

From 2.25 it is possible to calculate the localised surface plasmon frequency:

$$\omega_{LSP} = \frac{\omega_p}{\sqrt{1 + 2\varepsilon_m}} \tag{2.26}$$

The classical electromagnetic enhancement generated by the local surface plasmon is expressed as:

$$\mathbf{E}_{LSP} = \frac{\varepsilon - \varepsilon_m}{\varepsilon + 2\varepsilon_m} \frac{a^3}{(a+d)^3} \mathbf{E}_0 \tag{2.27}$$

Being d the distance between the analyte molecule and the surface of the nanoparticle.

Actually, to evaluate the enhancement it's more convenient to consider $\mathbf{E}_{LSP} >> \mathbf{E}_0$, and evaluate an enhancement factor, defined by:

$$A(\omega) = \frac{\mathbf{E}_{TOT}}{\mathbf{E}_0} \approx \frac{\mathbf{E}_{LSP}}{\mathbf{E}_0} = \frac{\varepsilon - \varepsilon_m}{\varepsilon + 2\varepsilon_m} \frac{a^3}{(a+d)^3} \tag{2.28}$$

Eq. 2.28 represents the enhancement in the electric field felt by the analyte molecule. It is evident the strong dependence of the enhancement factor $A(\omega)$ on the analyte-nanoparticle distance. If the analyte molecule is not close enough to the nanoparticle (i.e., large d values) the electromagnetic enhancement dramatically decreases. The SERS electromagnetic enhancement is obtained by considering both the incoming excitation and the scattered radiation:

$$I(\omega) = |A(\omega_S)|^2 |A(\omega_L)|^2 \approx \left| \frac{\varepsilon(\omega_S) - \varepsilon_m}{\varepsilon(\omega_S) + 2\varepsilon_m} \right|^2 \left| \frac{\varepsilon(\omega_L) - \varepsilon_m}{\varepsilon(\omega_L) + 2\varepsilon_m} \right|^2 \frac{a^{12}}{(a+d)^{12}} \tag{2.29}$$

where subscripts, S and L stand for Stokes and Laser.

Thanks to this model, enhancement factors of about 10^6 can be justified. For higher enhancement, that have been observed, the concept of hot spots was introduced. The hot spots are particular sites between two nanoparticles placed at a certain distance. It has been demonstrated that the electric field in the junction is not just the linear superposition of the contributions from the two nanoparticles, but it is more intense since coupling of higher order dipole moment comes into play. In this case the enhancement depends on the dimension of the nanoparticles, on their distance, and on the polarization of the incoming light. This situation is possible, for example, on nanostructured surfaces that allow the hot spot formation, as the one used in this thesis work.

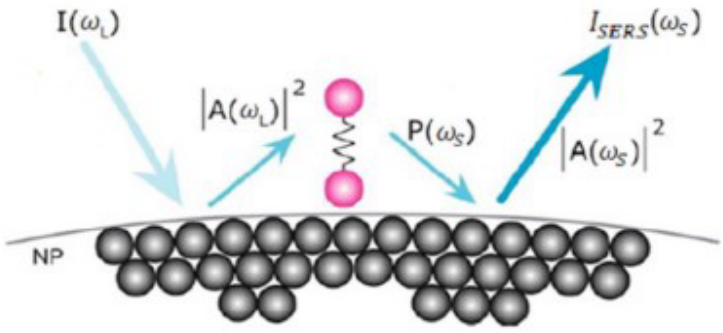

Figure 2.2: Schematic representation of the electromagnetic enhancement [27].

2.2.3. Chemical enhancement

An additional contribution to the global enhancement in a SERS experiment is also provided by the chemical enhancement. This contribution originates from any modifcation of the polarizability of a molecule due to the chemical-physical interaction with the substrate. This kind of enhancement strongly depends on the molecule and requires direct adsorption, thus a smaller contribution to the total intensification take place (10^2 - 10^4) [21].

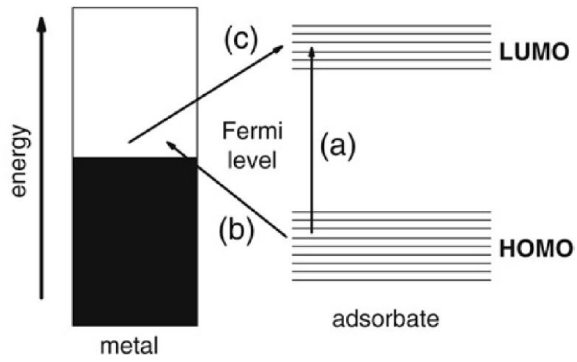

Figure 2.3: Energy level diagram for a molecule-metal complex [6].

Several mechanisms have been investigated and the debate is still not concluded. However, the so-called charge-transfer mechanism is one of the most probable effects and can be involved in different ways depending on the specific chemical configuration [6]:

- Type I acts on not-bonded analyte molecules. The weak van der Waals forces are responsible for a slight perturbation of the geometrical and electronic structure of the molecule, leading to a small modification of the Raman polarizability.
- Type II occurs when a metal-adsorbate complex is formed. Because of the electronic coupling and the overlap of molecular orbitals, new electronic states and new indirect transitions appears. This produces a considerable modification of the molecular polarizability. This effect is even stronger when the new electronic states are in resonance with the excitation laser.
- Type III involves photo-driven charge transfer between the molecule and the metal. It occurs when the energy difference between the Fermi level of the metal and the HOMO/LUMO of the molecule is matched by the exciting radiation.

We can identify chemical enhancement as the generation of resonant energy levels due to the interaction between the analyte with the nanostructured metallic surface. The intensity due to chemical enhancement depends proportionally on the number of absorbed molecules, N_{ads}, and on the Raman cross section, σ_{ads}, of the adsorbate:

$$I(\omega_s) \propto N_{ads}\sigma_{ads} \tag{2.30}$$

The evaluation of the chemical contributions to the SERS enhancement is very difficult and additional factors such as the molecule orientation and the presence of ions in the electrolyte should be considered. Computational methods like DFT and molecular dynamics

can be used to provide a theoretical justification [6, 21].

2.3. UV-Vis optical spectroscopy

Ultraviolet-visible spectroscopy exploits molecular absorption of radiation in the UV-VIS range (approximately between 190 and 800 nm) for the identification of organic and inorganic compounds, for the characterization of samples and for quantitative analysis on solutions and gases [4]. UV and VIS photons have enough energy to promote transitions between electronic states and information about the electronic structure of a compound can be gained. Selection rules can help one predict which transitions are allowed or forbidden. The inspection of UV-Vis spectra allows the investigation of the effect of molecular geometry, functional groups and solvent on electronic transitions, especially when organic species are considered. In addition, UV-Vis spectroscopy is a common technique to probe the plasmonic behaviour of metallic colloids, highlighting the resonance frequency for absorption and scattering.

2.3.1. Transmission UV-Vis

In transmission configuration, polychromatic radiation emitted by two separate sources (typically, a halogen lamp for the visible component and a deuterium lamp for the UV component) passes through a transparent cuvette containing the sample. In order to compensate for reflection losses and absorption by the cuvette and the solvent, the transmitted beam is compared at the detector with a beam emerging from a reference cuvette containing the solvent only. After proper corrections and subtractions, the absorption spectrum as a function of wavelength is provided in terms of absorbance (A), defined by equation 2.31:

$$A = -\log(T) = \log\left(\frac{I_0}{I}\right) \tag{2.31}$$

where T is the transmittance, I_0 is the incident intensity and I is the intensity attenuated by the sample. The absorbance can be empirically correlated to the molar concentration C of the absorber by the Lambert-Beer's law:

$$A = \varepsilon_\lambda C l \tag{2.32}$$

where ε_λ is the molar extinction coefficient and l is the optical path during which attenuation occurs.

2.4. Instrumentation

2.4.1. Dispersive Raman LabRAM HR800

The Horiba Jobin Yvon LabRAM HR800 Raman spectrometer was used to collect all the spectra reported in this work (Figure 2.4).

Figure 2.4: Image of LabRAM HR800.

It has been used in combination with two different laser radiations:

1. 633 nm from a HeNe laser in SERS experiments.
2. 785 nm (NIR) from a solid-state laser (laser XTRA, Toptica Photonics) in Raman measurements.

The lasers power can be modulated from the nominal value up to 10^{-4} its nominal value, through a series of filters with different optical densities.

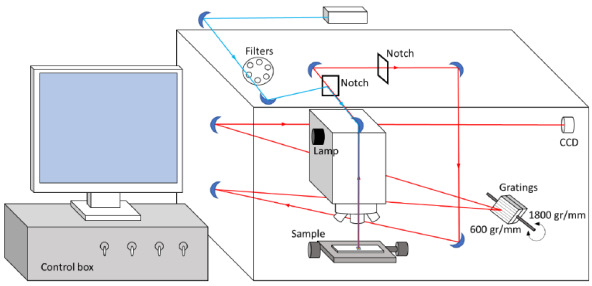

Figure 2.5: LabRAM HR800 internal configuration for 785 and 633 nm excitation [22].

In figure 2.5 it is possible to see all the major features of the spectrometer. The optical part is provided by an Olympus BX41 microscope equipped by 10x, 20x and 50x objectives and a camera for visual inspection. The laser, through a series of mirrors, initially arrives to an interference filter used to remove spurious spectral lines. Then, after the interaction of

light with the sample, an edge filter (or a notch filter for 785 or 633 nm excitation) removes the Rayleigh component of the scattered light. After that, the Raman scattered radiation travels toward a grating that can have two configurations: 600 gr/mm and 1800 gr/mm. The radiation dispersed by the grating is directed to a CCD (charge-coupled device) detector. It is cooled by a Peltier cell and has an operational temperature around -65°C. Finally, the Raman signal is processed by a computer dedicated software (*LabSpectra*).

2.4.2. Spectrophotometer UV-Vis JASCO V-570

The instrument features two deuterium and halogen lamps which cover the whole spectral range of measurement, emmitting radiation on UV and VIS-NIR, respectively.

Figure 2.6: JASCO V-570 UV-Vis spectrophotometer [27].

A spherical mirror selects the source that illuminates the entrance slit of the monochromator, sending the radiation on a plane mirror that further leads the light on the filters. The two slits are variable in width and height and the Czerny-Turner monochromator exploits two disperding gratings with a switch at $800 - 900$ nm to cover the whole spectral range. Then the radiation is reflected to reach a splitter that separates it in two components that will intecept the sample and the reference. The radiation is collected and reaches the detector, which is a photomultiplier for UV or PbS for NIR. The detector see in succession the sample signal, then the reference and the dark which are subtracted. The signal is then elaborated by the software to give the requested information as absorbance, trasmittance or reflectance. For the analyte solutions, quartz cells of 1 cm width have been used, changing the reference sample properly.

3 | Materials

3.1. Perampanel (PER)

Perampanel is a novel, highly selective, orally active, non-competitive AMPA receptor used for the treatment of epileptic seizures. It was identified through a targeted research program at Eisai Research Laboratories [25]. Its IUPAC name is 2-(2-oxo-1-phenyl-5-pyridin-2-yl-1,2-dihydropyridin-3-yl) Benzonitrile, and its chemical structure is depicted in figure 3.1.

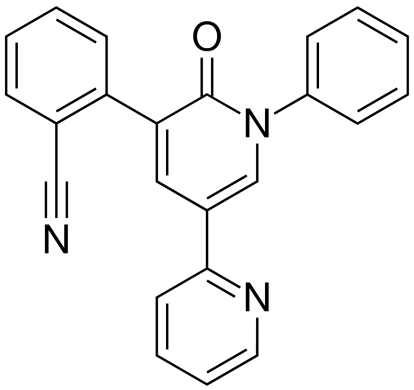

Figure 3.1: Chemical structure of Perampanel (PER).

To discuss SERS experiments, it is of paramount importance to characterize the Raman spectrum of the molecule. Therefore, Raman spectroscopy was used in order to detect the vibrational modes of PER and identify them as markers of PER so that the PER molecule could be recognized in subsequent SERS measurements.

Therefore, Raman measurements were made on solid PER powder. The Raman spectrum is depicted in figure 3.2.

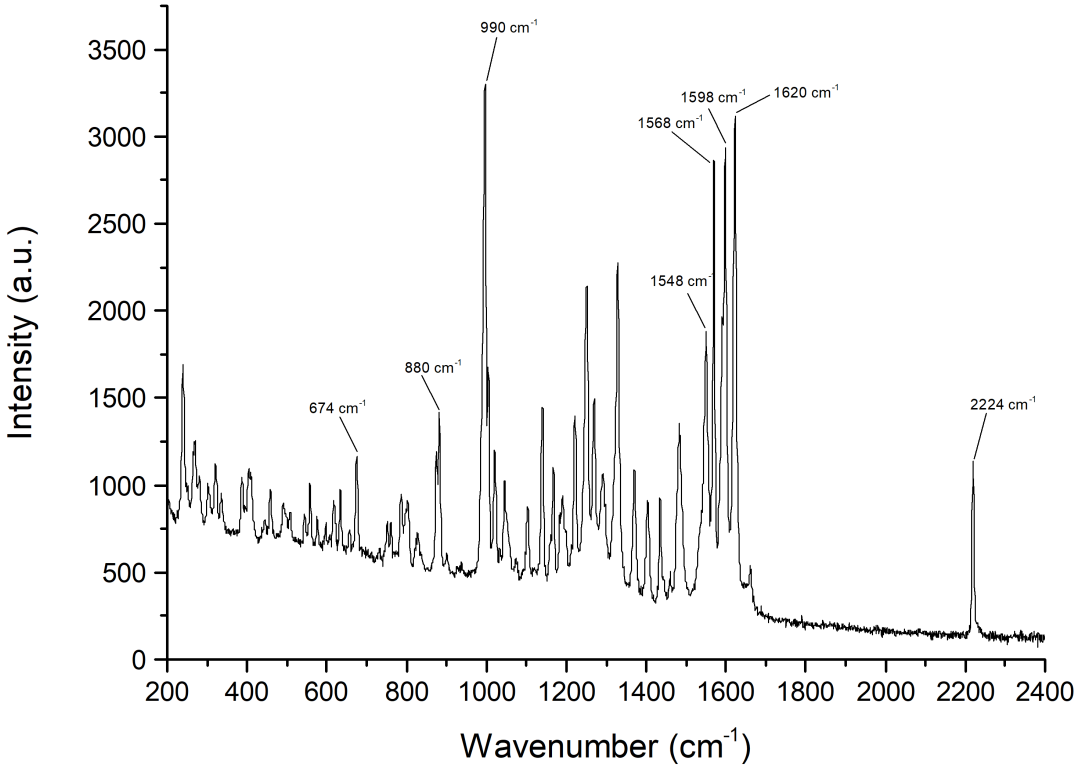

Figure 3.2: Raman spectra of solid PER. Spectrum collected with using 785 nm laser excitation, 30 mW power, 30 seconds exposition time, 3 averages. For further experimental details see section 3.4.

Based on Density Functional Theory calculations (DFT B3LYP/6-31G(d,p)), the main vibrational modes of PER were assigned, as reported in table 3.1

Wavenumber (cm^{-1})	**Mode**
670	In-plane C-H bending
875	Out-of-plane C-H bending
990	Ring breathing
1548, 1568, 1596, 1598, 1620	Aromatic ring stretching modes
2224	C≡N Stretching

Table 3.1: List of the main vibrational modes of PER [27] [16].

Peaks at wavenumbers of 670, 875, 990, and 2224 cm^{-1}were chosen as markers of PER,

these will be reported directly in the spectra present in this thesis. These peaks were chosen as markers because they are also shown to be present in the SERS spectra of solutions at low concentrations of PER [8].

3.2. SERS substrates

Noble metal nanoparticles are widely used as a material for the production of SERS substrates. The ability to create nanostructured films with variable morphologies that affect the optical properties of the substrates makes materials such as gold of particular interest for this type of use. It is possible to produce highly selective and sensitive substrates. In this thesis, glass substrates decorated with a film of Au nanoparticles produced and deposited by PLD were used. The process took place at the *CNR-Instituto per i Processi Chimico-Fisici* in Messina and is described in a previous thesis [22].

The deposition process is based on the evaporation of a rotating target of pure gold, which is hit by a high-intensity laser and generates a plasma feather of vaporized Au atoms that is deposited on the rotating glass substrate.

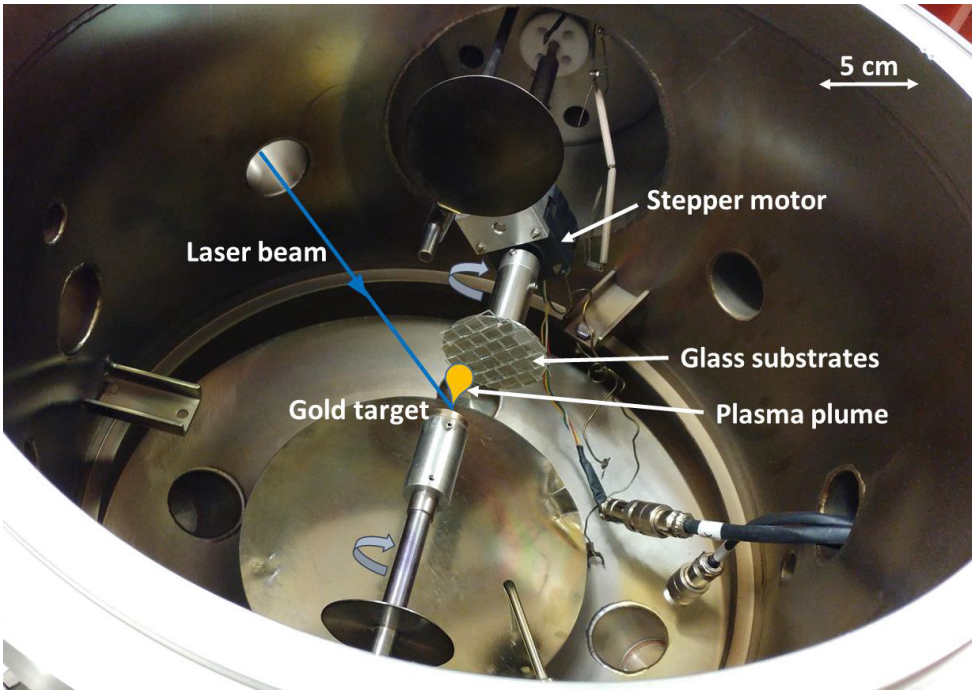

Figure 3.3: Deposition chamber set up.

The apparatus is placed in a vacuum chamber filled with Ar gas to promote collisions between the species present in the plasma feather. Typically, nanoparticles with a diameter between 2-20 nm are obtained. it has been observed that the morphology of the

deposited film depends on the number of laser pulses (N_{LP}). In particular above 30000 (N_{LP}) the deposited film exhibits a bilayer structure where on the first percolated layer there is a second layer of isolated spherical nanoparticles [1]. In figure 3.4 the image of the surface of substrate no.27, taken with the scanning electron microscope (SEM) at the Department of Energy of the Politecnico di Milano.

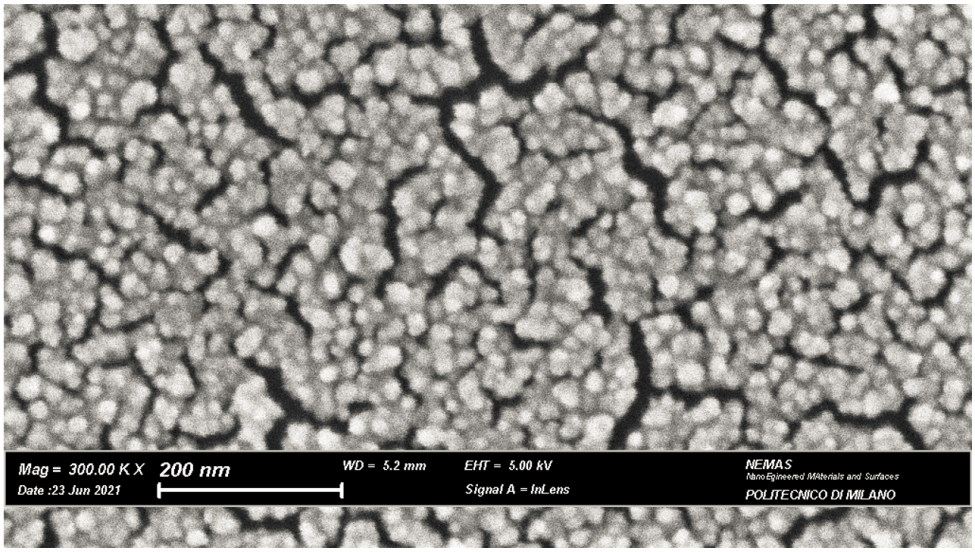

Figure 3.4: SEM images highlighting the morphology of the Au substrates deposited at 100 Pa of Ar with 35000 laser pulses.

It has been shown through numerical simulation that the hot spots, the places where the SERS amplification effect is greatest, are located in the nanochannels that separate islands. For this reason, percolated structures are of interest. These allow for preferential adsorption sites for molecules. Smaller molecules such as drug molecules are preferentially adsorbed in the channels between the islands, which usually have a width of about 20 nm, while molecules with higher molecular weight such as proteins and lipids adsorb on the surface of the nanoparticle islands. The substrates were characterized at *CNR-Instituto per i Processi Chimico-Fisici* in Messina by UV-Vis spectroscopy to identify the location of SPR. Figure 3.5 shows the SPR values for the batch of substrates produced.

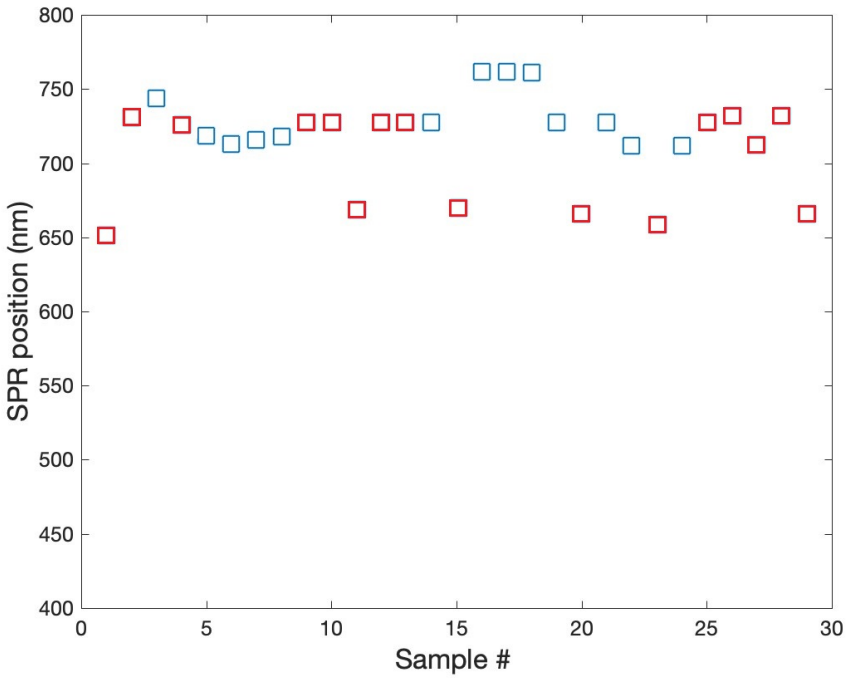

Figure 3.5: SPR position of the batch of SERS substrates used in this thesis work, the substrates used in the experiments of this thesis are highlighted in red.

The SPR value are in a range between 650 and 725 nm. Therefore, in order to maximize the enhancement of the Raman signal, I chose to use a He-Ne laser that emits at 633 nm.

3.3. Solutions

The chemical agents used in this thesis are as follows:

- Solid PER Eisai Co.,Ltd. (ER-No. ER-155055-90; Lot No. 173H2901).
- Methanol 99.5% (CAS:57-56-1, *Sigma-Aldrich*).
- Hydrochloric acid 37% (CAS:7647-01-0, *Sigma-Aldrich*).
- Sulfuric Acid 96% (CAS:7664-93-9, *Carlo Erba*).
- Chloroform $99 - 99.4\%$ (CAS:67-66-3, *Sigma-Aldrich*).

During this thesis work, several solutions were prepared and used as the basis for the preparation of solutions analyzed by SERS spectroscopy. The solutions with their compositions are shown in the tables 3.2 and 3.3.

Solution Name	Description	PER	Methanol
A	Solution of PER diluted in methanol 10^{-3} M	1 mg	3 ml
B	Solution of PER diluted in methanol 10^{-2} M	3.49 mg	1 ml

Table 3.2: PER solutions recipies.

Solution Name	Description	Distilled water	Solforic acid	Cloridric acid
C	Acid solution pH=2	500 ml	0.251 ml	41 μl
D	Acid solution pH=0	50 ml	2.783 ml	—

Table 3.3: Acid solutions recipies.

3.4. Typical experimental setup of SERS and Raman measurements

Unless otherwise specified, I adopted the following procedures for sample collection, preparation, and spectroscopic measurements during this thesis.

- Saliva collection. Whole saliva is collected by spitting into a test tube. Sampling takes place on the same day as the measurement in the unstimulated condition (US)(see section 4), at least one hour after meals.
- Preparation of the analyte. Perampanel was supplied in powder form so it was necessary to solubilize it with methanol which is a good solvent up to concentrations of 10^{-2} M. Two solutions of PER diluted in methanol were prepared, solution A and B (see section 3.3). Small volumes of solution A or B are diluted in saliva. To prepare a sample suitable for SERS analysis the PER is protonated by adding to solution A or B diluted in saliva a certain amount of solution C or D (see section 3.3) in order to bring the final solution to the desired pH value.
- Raman spectroscopy. The analyte is placed on a slide covered with aluminum foil, if it is liquid state analyte it is first air dried. A 785 nm or 633 nm laser, focused through a 50x objective, was used as the excitation source. The laser power, exposure time, and number of averages vary depending on the experiment and are reported on a case-by-case basis.

- SERS Spectroscopy. An analyte droplet of approximately 1-2 μl is deposited on the SERS sensor and air-dried. A 633 nm laser, focused through a 50x objective, was used as the excitation source. The laser power is 0.3 mW, the exposure time and number of averages varies depending on the experiment and are reported on a case-by-case basis.

4 | Saliva

4.1. Saliva

Saliva is a clear, slightly acidic mucous exocrine secretion present in the mouth. It is produced by the major and minor salivary glands and crevicular gingival fluid [10]. Saliva has several functions involved in oral health and homeostasis. It plays a role in maintaining oral health. Saliva aids in bolus formation by moistening the food [18], protects the oral mucosa against mechanical damage, and plays an active role in the preliminary digestion of food due to the presence of enzymes contained in it [29]. Other functions of saliva include lubrication of the oral cavity, maintenance of mucosal integrity, remineralization, growth factor and antimicrobial function [12].

The study of saliva as a biological fluid for AED TDM was introduced in the 1970s. The most studied drugs in this regard are phenytoin, phenobarbital, and carbamazepine [5]. Saliva is emerging again as a biological fluid of interest for AED TDM and has begun to be increasingly used given its advantages over serum or blood. The drug concentration in saliva generally reflects the percentage of pharmacologically active drug that has not bound to proteins in the serum, in addition, sampling is much simpler and easier, the presence of a trained operator is not required, and stress on the patient is minimized [20]. This allows for a cost-effective approach to screening large populations. However, the use of saliva as a fluid for TDM also has some disadvantages: the results obtained can be affected by contaminants present in the saliva such as residues of other drugs or food, the volume of saliva that can be collected may be insufficient to perform clinical tests, and the viscosity of saliva can cause problems during pipetting [20].

Migration of compounds such as drugs from plasma to saliva can occur by several mechanisms:

- Ultrafiltration occurs through the junctions between cells of secretory units (intercellular nexus). Only molecules with a molecular weight below 1900 g/mol are involved (water, ions and hormones such as catecholamines and steroids) in this type of process. Their concentration in saliva results to be $300 - 3000$ times lower

than the concentration in plasma [2].

- Transudation of the compounds present in the plasma into the oral cavity, through the crevicular fluid or directly from the oral mucosa. The presence in saliva of some typical plasma molecules, such as albumin, depends on this mechanism [2].
- Selective transport across cell membranes: by diffusion of lipophilic molecules such as steroid hormones or by active transport through protein channels [2].

4.2. Saliva sampling

Standardization of salivary specimen collection is of great importance in saliva analysis since several factors can affect flow, salivary composition and pH. Whole saliva, saliva from the glandular duct, crevicular fluid, and mucosal transudate are samples that can be obtained from oral fluid following specially designed collection methods specific to each. Among these, the most repeatable and easy to obtain sample is whole saliva [3].

Whole saliva can be divided into unstimulated (US) and stimulated saliva (SS) depending on the method of collection. Unstimulated whole saliva (US) can be collected by different collection methods such as by passive drooling, without any oral movement, where saliva is allowed to drain from the lower lip into a vial. Or, by spitting directly into a collection vial [19]. Stimulated whole saliva (SS) can be obtained by oral movements such as gentle chewing or by using citric acid, placed on the tongue, to stimulate its production [3].

In this thesis work, I chose to use my own saliva to carry out the experiments. This choice is due to the fact that I am auto-immune to my own saliva. This minimizes the biological risk of handling saliva during sample preparation. Saliva was collected under unstimulated conditions by spitting into a test tube where it was collected.

4.3. Saliva charaterization

4.3.1. Raman spectroscopy

In order to discuss the SERS measurements made during this thesis, it is necessary to characterize saliva by Raman spectroscopy. The requirement is due to the need to know the Raman response of saliva in order to discern the contribution of saliva from that of the PER. In addition, knowledge of the components of saliva is necessary to evaluate possible interactions between them and the drug.

Saliva samples were taken according to the procedure outlined in section 3.4, on five

different days, during different times of the day: after breakfast, mid-morning, and late afternoon, in order to verify the reproducibility of the Raman response of the samples.

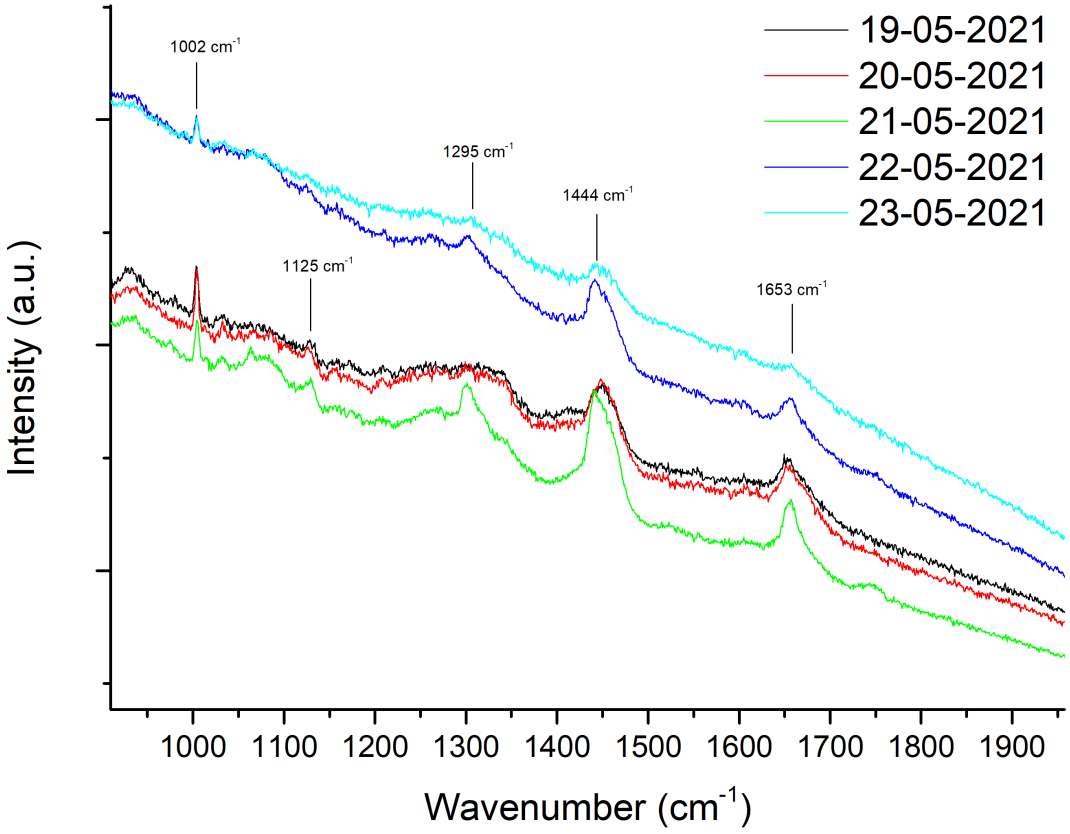

Figure 4.1: Spectra of dryed saliva samples taken in five different days. Spectra were collected on an aluminum foil substrate, using 785 nm excitation, 50x objective, 1 mW power, 30 seconds exposure time and 3 averages

Given the results of the measurements shown in figure 4.1 it is possible to state that the Raman signal of saliva is highly reproducible. No significant changes are noticed in the spectra of the samples, even though they were taken on different days and at different times of the day.

The assignement of the main Ramna peaks of saliva samples are listed in table 4.1.

Wavenumber (cm^{-1})	Vibrational modes	Associated molecule
1744	C=O stretching	acetates
1653	—	ammide I
1444	CH stretching	glycoprotein
1434	CH_2 bending	acetates
1295	C−O stretching	acetates
1265	Sym. ring deformation	Tyrosin
1125	CH_3 rocking	—
1120	C−C stretching	—
1097	C−O stretching	—
1047	C−CH_3 vibration	—
1002	ring breathing	fenilanin
991	uncertain	—
927	CH bending	—
919	uncertain	—
852	C−N stretching	—
632	skeletal bending	—
544	C−CH_3 bending	—

Table 4.1: Assignement of the contributions in the saliva spectrum [23, 28].

Peaks at 1005, 1063, 1129, 1300, 1440 and 1656 $cm^{-1}$are clearly visible in almost all spectra (Figure 4.1), and these same signals are also found in the literature [23, 28]. With the exclusion of the signal at 1005 cm^{-1}none of the other peaks typical of the Raman response of saliva overlap with the PER markers (see section 3.1). We can then proceed with the experiments on PER in saliva in the certainty that the signal of saliva does not interfere with that of PER during SERS measurements.

4.3.2. Saliva pH and its buffer capability

The importance of the pH value of the solution on which measurements are made has been demonstrated in previous theses [27]. To increase the response of PER it is necessary to protonate it. To make this happen, solution C is used and mixed with solution A or B in order to bring the final solution to a pH value between 2 and 4. For this reason it is necessary to characterize the pH value of saliva and its behavior when interacting with

acidic solutions.

The solutions with their compositions are shown in the tables 4.2 and 4.3.

Solution Name	Description	PER	Methanol
A	Solution of PER diluted in methanol 10^{-3} M	1 mg	3 ml
B	Solution of PER diluted in methanol 10^{-2} M	3.49 mg	1 ml

Table 4.2: PER solutions recipies.

Solution Name	Description	Distilled water	Solforic acid	Cloridric acid
C	Acid solution pH=2	500 ml	0.251 ml	41 μl
D	Acid solution pH=0	50 ml	2.783 ml	—

Table 4.3: Acid solutions recipies.

Unstimulated whole saliva in a healthy individual has a pH ranging between 6.25 and 7 [7]. To verify that the pH of my saliva was consistent with the data in the literature and to check for variability, three pH measurements were made on different samples using litmus paper. Samples were taken on different days and times of the day.

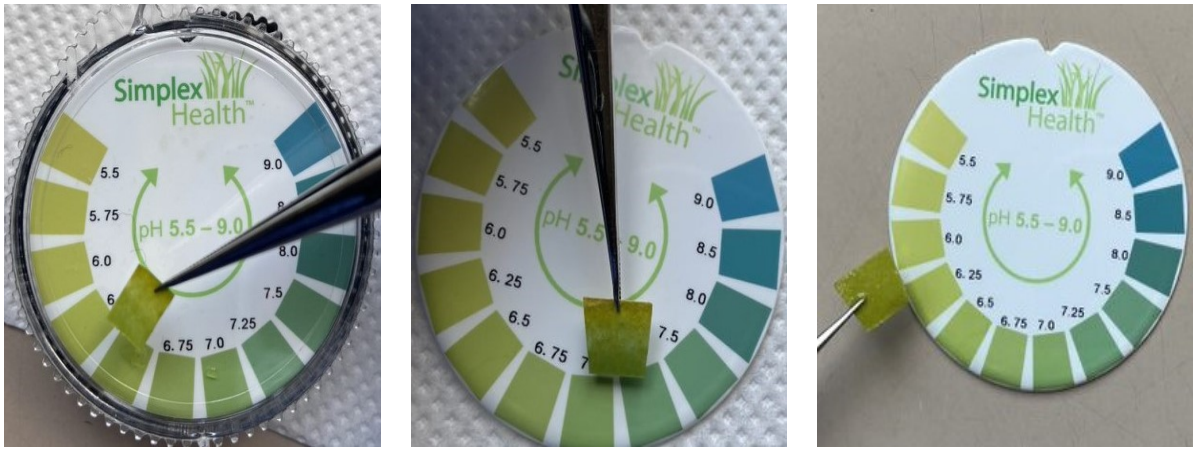

(a) *Sample take 18/05/21 morning, pH= 6.25/6.75*

(b) *Sample take 17/05/21 afternoon, pH= 6.75/7.25*

(c) *Sample take 17/05/21 morning, pH= 6.25/6.5*

Figure 4.2: Meausurements of the pH on three different saliva samples .

The measured pH varies between $6.25 and 7$ (Figure 4.2), these values are in agreement

with those reported in the literature [7]. Furthermore, the pH values are quite similar for all three samples. This allows us to state that the pH of saliva does not vary significantly between samples. Therefore, the pH can be considered constant in the range of pH 6.25 to 7 for all samples taken in the future.

US saliva possesses three separate buffering systems that provide it with a total buffering capacity of approximately 5.93 mmol H^+/l [7]. The first buffer is based on bicarbonate chemistry and contributes incira to 80% of the buffering capacity. The second and third buffers, on the other hand, are based on proteins contained in saliva and phosphates, respectively.

A titration experiment was performed to get familiar with the actual buffering capacity of saliva. Controlled volumes of solution C were added step-wise to a volume of 1 ml of saliva. After each addition the pH of the solution was measured with a litmus paper.

Saliva:C volume ratio	**pH**
Saliva	$6-7$
1 : 2	5
1 : 4	4
1 : 6	3
1 : 7	3
1 : 8	$3-2$
1 : 9	~ 2
1 : 10	2
C	2

Table 4.4: Saliva and solution C Volume ratios and realtive pH values in the titration experiment.

Figure 4.3: Measures of the pH of the solutions at differents volume ratios.

The titration experiment shows that it is necessary to work with at least a 1:9 volumetric ratio of saliva to C to bring the solution to pH 2 which is the optimal value for SERS measurements of PER [27].

5 | Detection of PER by SERS: direct measurements on saliva

5.1. Direct measurements on saliva

The first attempt to detect diluted PER in saliva through SERS was conducted as follows. 10 μl of A was diluted with 10 μl of saliva and then the solution was acidified by adding 80 μl of C. The final PER concentration in the solution was found to be 10^{-4} M. The procedure by which the measurement was made is described in section 3.4.

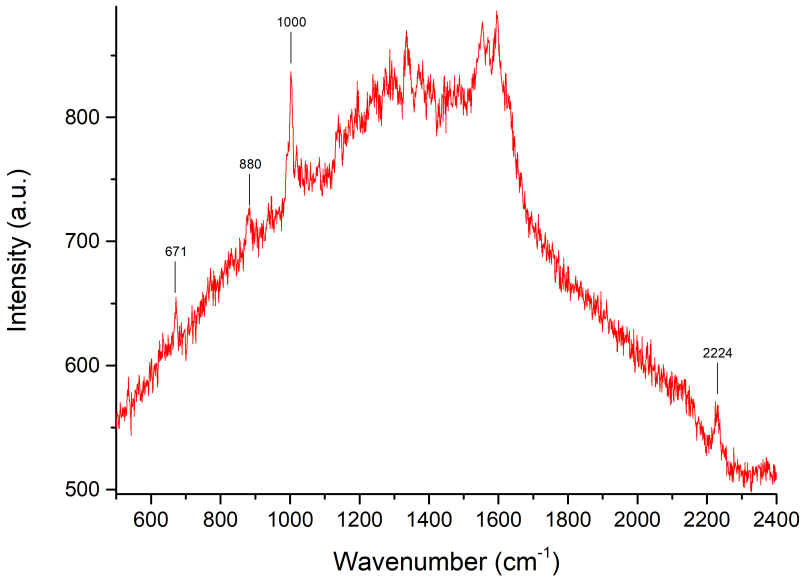

Figure 5.1: SERS measurements of PER diluted in saliva in acidic condition. Collected on SERS substrate n.1, using 633 nm laser excitation, 50x objective, 0.3 mW power, 60 seconds exposure time and 3 averages.

As can be seen from the figure 5.1, the signal of the PER can be clearly distinguished. In particular we can see that the peaks at 671, 880, 1000 and 2224 cm^{-1}, which were

chosen as markers of the drug (see section 3.1), are present in the spectrum and well distinguished from the background noise. This demonstrates that it is possible to detect diluted PER in saliva.

A detection test of Perampanel at lower concentrations was done by preparing five solutions of PER diluted in saliva and then acidified. The preparation process was as follows: A was diluted in a 1:1 volumetric ratio with saliva. Then the resulting solution was divided into five parts of 10 μl that were acidified by adding volumes of solution C so that the desired PER concentration was achieved. The prepared solutions ranged in concentration from 10^{-4} M up to 10^{-6} M. The volumetric composition of the solutions is shown in Table 5.1.

Sol. A diluted in saliva	Sol. C	PER concentration
10 μl	40 μl	10^{-4} M
10 μl	90 μl	5×10^{-5} M
10 μl	490 μl	10^{-5} M
10 μl	990 μl	5×10^{-6} M
10 μl	4990 μl	10^{-6} M

Table 5.1: Recipes of the different solutions containing PER that have been tested with SERS spectroscopy.

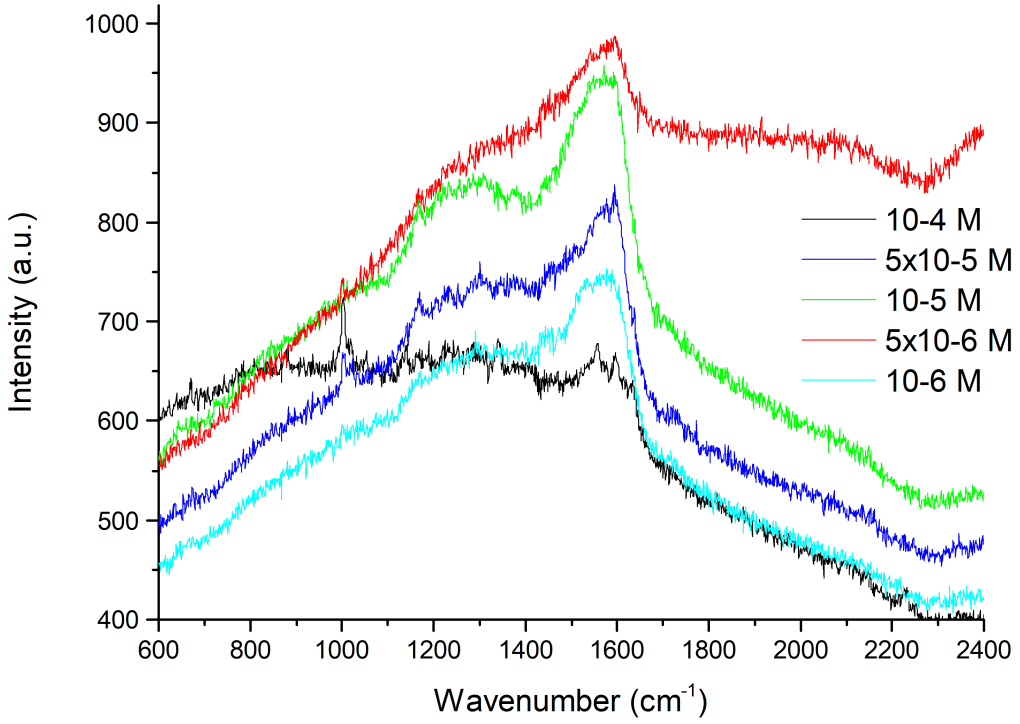

Figure 5.2: SERS measurements of PER diluted saliva in acidic condition. Collected on SERS substrate n.20 and n.11, using 633 nm laser excitation, 50x objective, 0.3 mW power, 60 seconds exposure time and 10 averages.

From the SERS analysis (Figure 5.2) it can be seen that the main markers of PER are visible only in the solution with concentration 10^{-4} M. Going down with the concentration of PER the markers are no longer visible. In addition, we note the presence of a fluorescence band between $1500 - 1600$ cm^{-1}that hides the Perampanel signals in that area of the spectrum. A possible explanation for the failure to detect PER at lower concentrations of 10^{-4} M can be attributed to the fact that the prepared solutions are composed mostly of solution C . This problem stems from the high buffering power of saliva that forces to use large volumes of solution C in order to be sure to acidify the PER.

To solve this problem it was decided to change the solution used to acidify the PER. The acidifying solution used from now on will be solution D that, with its low pH value, allows to break the buffer system of saliva by adding small volumes of solution. The choice to use only sulfuric acid comes from the fact that chlorine is already present in the saliva [9] and therefore the addition of hydrochloric acid would be superfluous.

5.1.1. Optimization of the analyte pH

Using a new acidifying solution (D), a preliminary study was done to see if there was any variation in the Raman response of PER solutions diluted in saliva as the pH varied.

Four different PER solutions were prepared in saliva at a fixed concentration of 10^{-4} M which were acidified with varying volumes of D solution to give pH values in the range of 2 to 5. The pH of the solutions was measured with a litmus paper. The composition of the solutions are shown in table 5.2.

Sol. A	Saliva	Sol. D	pH solution
20 μl	180 μl	2 μl	5
20 μl	180 μl	3 μl	4
20 μl	180 μl	4 μl	3
20 μl	180 μl	5 μl	2

Table 5.2: Recipes of the different solutions containing PER that have been tested with SERS spectroscopy in order to investigate the effect of the pH on the SERS reponse. All the solutions have a PER concentration of 10^{-4} M.

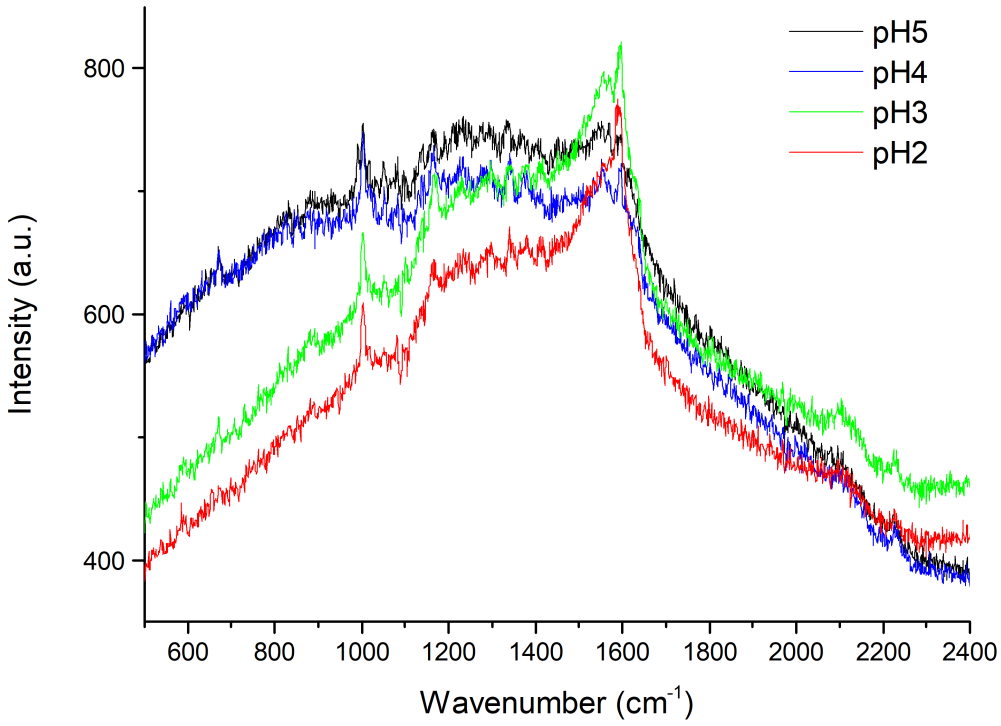

Figure 5.3: Spectra of the solutions (Tab. 5.2). Collected on SERS substrate n.29, using 633 nm laser excitation, 50x objective, 0.3 mW power, 60 seconds exposure time and 10 averages.

From the measurements in the figure 5.3, it can be seen that the fluorescence curve changes as the pH varies. In particular, passing from pH 4 to pH 3, we see that the fluorescence curve becomes very pronounced in the range between 600 and 1700 $cm^{-1}$and appears between 1500 and 1600 $cm^{-1}$the band already noted in previous measurements (Figure 5.2). Given these results it was decided to perform all subsequent measurements on acidified solutions at pH=4. At this pH value we are still certain that the PER is protonated [27] and at the same time we have a less intrusive fluorescence signal than at lower pH values.

5.1.2. Qualitative measurements of PER

Once the sample preparation was optimized (see section 5.1.1) the experiment to identify the PER diluted with saliva at lower concentration of 10^{-4} M was repeated. Four solutions were prepared by diluting solution A in saliva and acidifying the resulting solution with

negligible volumes of solution D so as to bring all solutions to pH=4. The pH measurement was done with a litmus paper. The composition of the solutions is shown in the table 5.3.

Sol. A	Saliva	Sol. D	PER concentration
20 μl	180 μl	3 μl	10^{-4} M
10 μl	190 μl	5 μl	5×10^{-5} M
10 μl	990 μl	7 μl	10^{-5} M
10 μl	1990 μl	17 μl	5×10^{-6} M

Table 5.3: Recipes of the different solutions containing PER that have been tested with SERS spectroscopy.

SERS measurements were made using the procedure outlined in section 3.4.

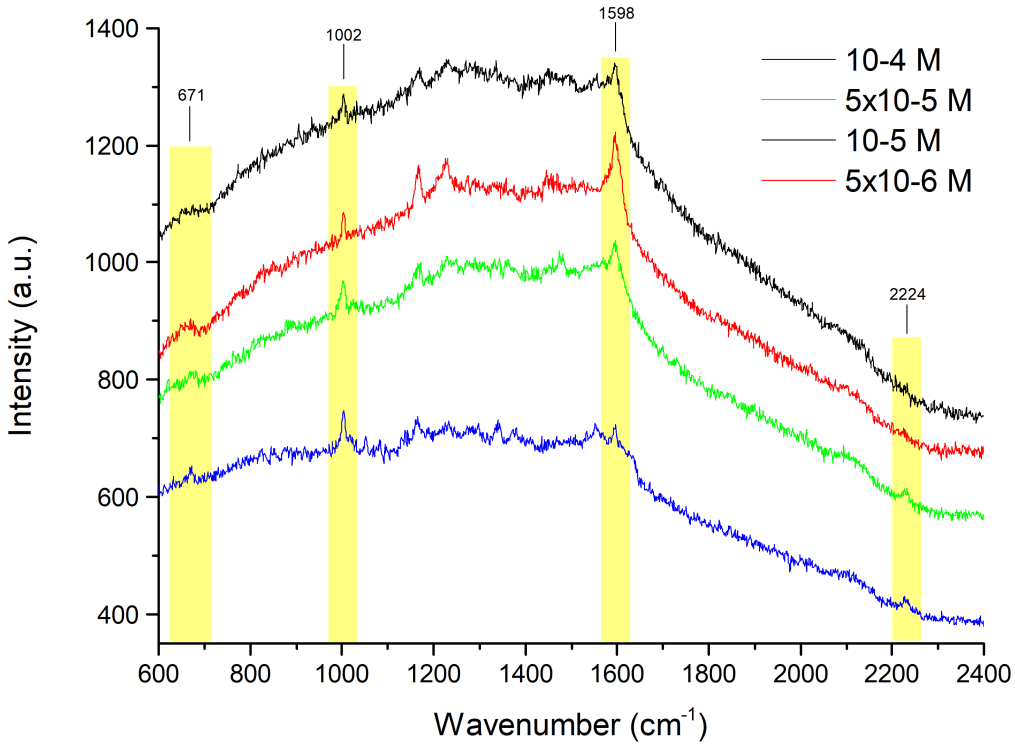

Figure 5.4: SERS measurements of PER diluted saliva in acidic condition (see Tab. 5.3). Collected on SERS substrate n.23, using 633 nm laser excitation, 50x objective, 0.3 mW power, 60 seconds exposure time and 10 averages.

The measurements show that it is possible to detect diluted Perampanel in saliva up to concentrations of 5×10^{-6} M. The main marker peaks of PER at 671 and 1002 $cm^{-1}$are visible in all solutions. Another typical PER peak at 1598 $cm^{-1}$is visible in all measurements. As demonstrated in previous theses [8, 16, 27] the peak at 2224 cm^{-1}disappears at low concentrations. In this case, at a concentration below 5×10^5 M, it no longer appears visible relative to the background noise.

5.2. Quantitative measurements of PER

To plot a calibration curve of the trend of the Raman response of PER as a function of concentration, four solutions at different PER concentrations were prepared. The concentration of the solutions are respectively 10^{-3}, 5×10^{-4}, 2.5×10^{-4} e 10^{-4} M.

Solution A or B was diluted in a variable volume of saliva that would allow the desired final concentration to be achieved. Next, the solution was acidified with negligible volumes of solution D so that the pH of the solutions was raised to 4. The pH was measured using a litmus paper. The composition of the solutions is shown in table 5.4.

Solution A or B	Saliva	Acid solution	Solution concentration
10 μl B	90 μl	0.6 μl	10^{-3} M
100 μl A	100 μl	1 μl	5×10^{-4} M
50 μl A	150 μl	1.1 μl	2.5×10^{-4} M
20 μl A	180 μl	1.2 μl	10^{-4} M

Table 5.4: Recipes of the different solutions containing PER that have been tested with SERS in order to do a quantitative measurement of the PER.

SERS measurements were performed using the procedure outlined in 3.4. For each sample, five measurements were made at five different spots in order to obtain an average value of the intensity of the SERS response of the sample.

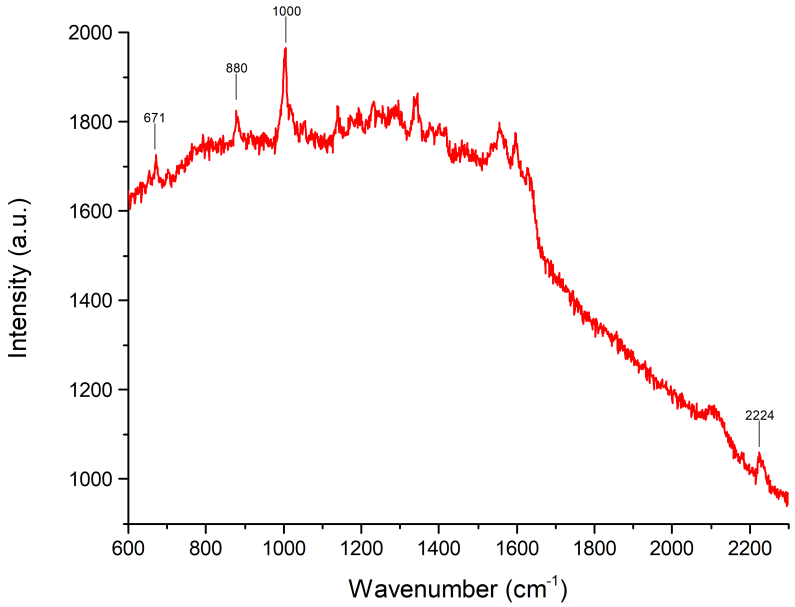

(a) *Solution with PER conc.* 10^{-3} *M.*

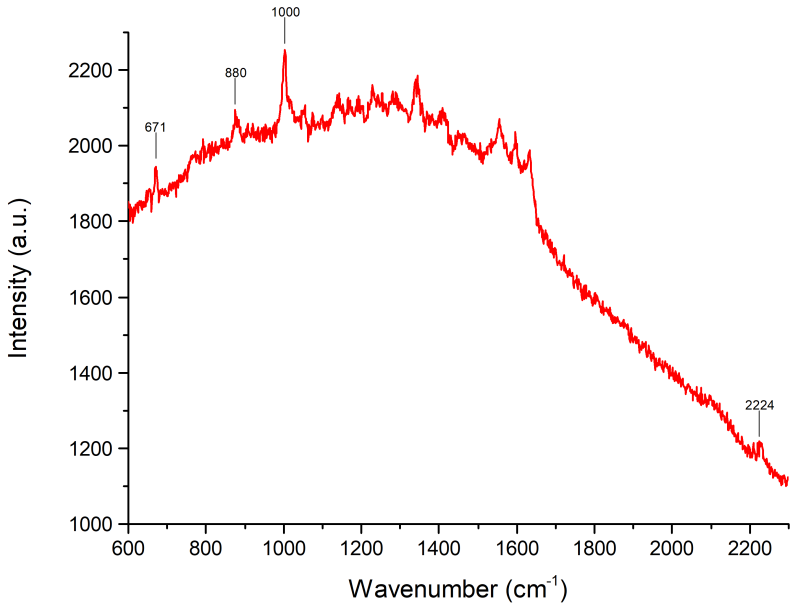

(b) *Solution with PER conc.* $5 \cdot 10^{-4}$ *M.*

Figure 5.5: Examples of the spectra of the solutions 10^{-3} and $5 \cdot 10^{-4}$ M. Collected on SERS substrate, using 633 nm excitation, 50x objective, 0.3 mW power, 120 seconds exposure time and 5 averages.

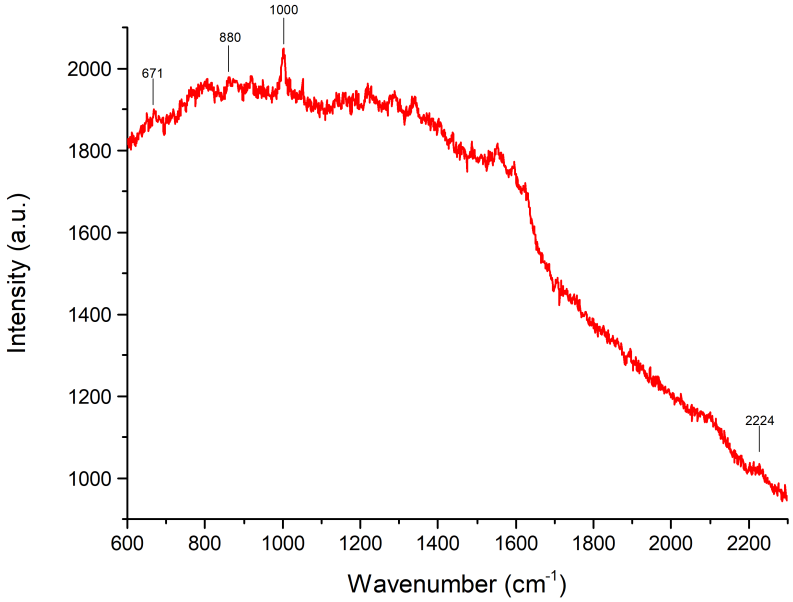

(a) *Solution with PER conc.* $2.5 \cdot 10^{-4}$ *M.*

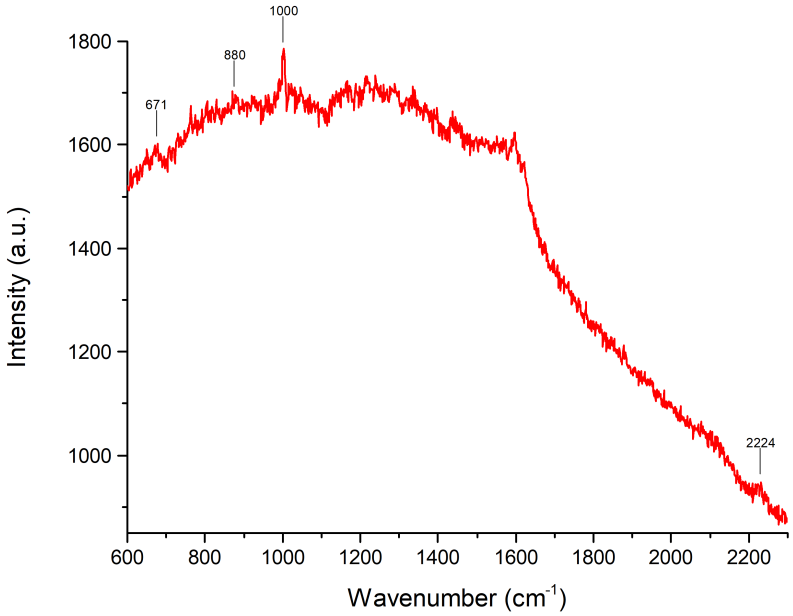

(b) *Solution with PER conc.* 10^{-4} *M.*

Figure 5.6: Examples of the spectra of the solutions $2.5 \cdot 10^{-4}$ and 10^{-4} M. Collected on SERS substrate, using 633 nm excitation, 50x objective, 0.3 mW power, 120 seconds exposure time and 5 averages.

The area underneath the PER marker peaks (see section 3.1) was calculated using the

related feature of the *Omnic* software. Data processing was performed using Excel. For each concentration, the area underneath the peaks was calculated as the average of the area measured over the five measurements made and related to the concentration. Error bars are defined as $\pm$ the standard deviation (σ). The values used to construct the calibration curves are given in table 5.5.

10^{-3} M	671 cm^{-1}	880 cm^{-1}	1000 cm^{-1}	2224 cm^{-1}
1	264	594	2104	777
2	651	720	2028	306
3	771	1342	2240	924
4	611	905	2198	907
5	427	811	2150	519
Average	545	874	2144	687
σ	200	285	83	267
5×10^{-4} M	671 cm^{-1}	880 cm^{-1}	1000 cm^{-1}	2224 cm^{-1}
1	445	957	2496	629
2	713	780	1670	584
3	553	756	1843	629
4	544	685	1314	622
5	465	888	1793	613
Average	544	813	1823	615
σ	106	109	429	19
2.5×10^{-4} M	671 cm^{-1}	880 cm^{-1}	1000 cm^{-1}	2224 cm^{-1}
1	350	638	1141	543
2	523	731	1267	477
3	658	555	1364	466
4	365	414	1272	398
5	357	497	1272	315
Average	451	567	1263	440
σ	136	123	79	87
10^{-4} M	671 cm^{-1}	880 cm^{-1}	1000 cm^{-1}	2224 cm^{-1}
1	351	435	1215	548
2	613	579	1591	566
3	381	574	1121	591
4	407	510	928	519
5	453	371	1000	491
Average	441	494	1171	543
σ	103	90	259	39

Table 5.5: Summary of the baseline corrected values of the area under each peak measured for PER concentrations of 10^{-3} M, $5{\times}10^{-4}$ M, $2.5{\times}10^{-4}$ M, 10^{-4} M. The corresponding averages and standard deviations are also reported.

The calibration curves of the four marker peaks of the PER are shown in Figure 5.7. Despite the non-negligible error bars, the average Raman response shows an increasing trend as concentration increases, which can be represented by linear curves with coefficients of determination (R^2) ranging from 0.66 to 0.92.

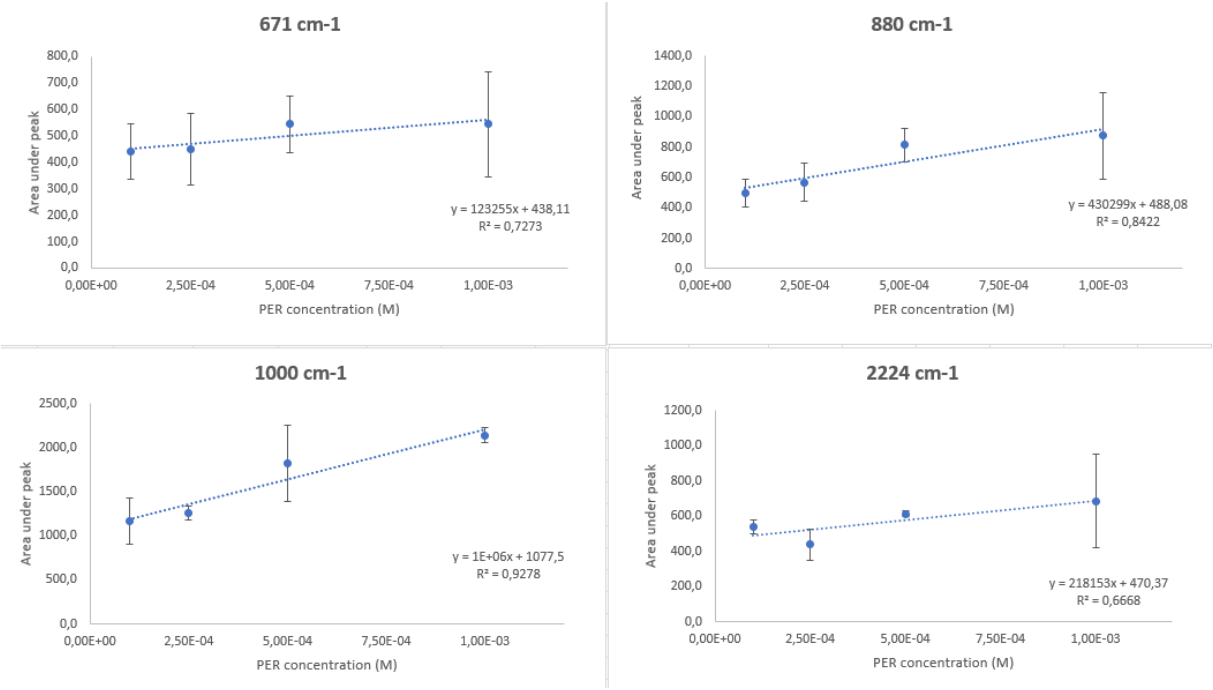

Figure 5.7: Calibration curves at four main PER peaks. The area under pea is plotted for any concentration and vertical error bars correspond to ± the standard deviations. The equation of the trendline and the coefficient of determination R^2 are also reported.

The data shown in figure 5.7 show a not negligible variability of the Raman response in the different points where the measurement was made at the same concentration and peak. These variations are underlined by the extension of the error bars and can be attributed to the fluorescence caused by the residues of some compounds present in the saliva that are deposited on the substrate. In addition, the relationship between the Raman response and the concentration of PER while being to a good linear approximation, does not converge to zero as the concentration of PER decreases, this is due to the presence of non-negligible background noise in the measurements caused by impurities present in the saliva.

In this section, the possibility of detecting PER in saliva and the possibility of plotting a calibration line of the Raman response as the drug concentration varies has been demonstrated. However, two issues arise from the measurements to date. The first is the background noise present in all measurements in the form of fluorescence that invalidates attempts to draw a line of accurate calibration. The second is the impossibility to work

at low concentrations of PER. Already at concentrations of 5×10^{-6} M the signal starts to be very weak. The real concentration of PER in the saliva of a hypothetical patient is around 10^{-9} M, a value far from the values of the concentrations under consideration.

An alternative method of analyte preparation must therefore be devised to overcome these problems.

6 | Detection of PER by SERS: pre-treatments of saliva samples

6.1. Pre-treatments of saliva samples

As reported in the previous section, the signal is distorted by an intense fluorescence signal which causes a high noise floor in the measurements. To make more accurate measurements, one can take advantage of an increase in laser power in order to increase the signal:noise ratio. However, increasing the irradiation power causes some problems. The nanoparticles deposited on the SERS sensor can sustain high irradiation power only for short periods. If they are exposed to such power for too long they become damaged. A possible solution to this problem is to use the spinning cell configuration pioneered in previous work. By spinning the substrate, the problem of thermal degradation is avoided since the single spot is irradiated by the laser for a small amount of time. However, the use of the spinning cell was not possible for the previous measurements since the solutions used so far, once dried on the SERS substrate, presented a thick layer of sediment composed of the high molecular weight components of saliva. This deposit gives rise to a strong fluorescence during measurements that makes the setup of the spinnig cell unusable.

It was therefore sought to find a way to eliminate the portion of saliva containing the high molecular weight species, which cause fluorescence in the measurements. These were the possibilities considered:

1. Filtration through cotton swab.
2. Centrifuge at 10000 rpm for 10 minutes.
3. Filtration through amorphous silica (63 μm grain size).
4. Phase separation using chloroform.

6.1.1. Centrifuge

I prepared a solution of 1 ml of solution A diluted in saliva with concentration 10^{-4} M and pH=4. 100 μl of A was diluted in 900 μl of saliva and subsequently acidified with 10 μl of D. The solution was centrifuged at 10000 rpm for 10 minutes and then the supernatant was collected. A drop of the supernatant was deposited on a SERS sensor.

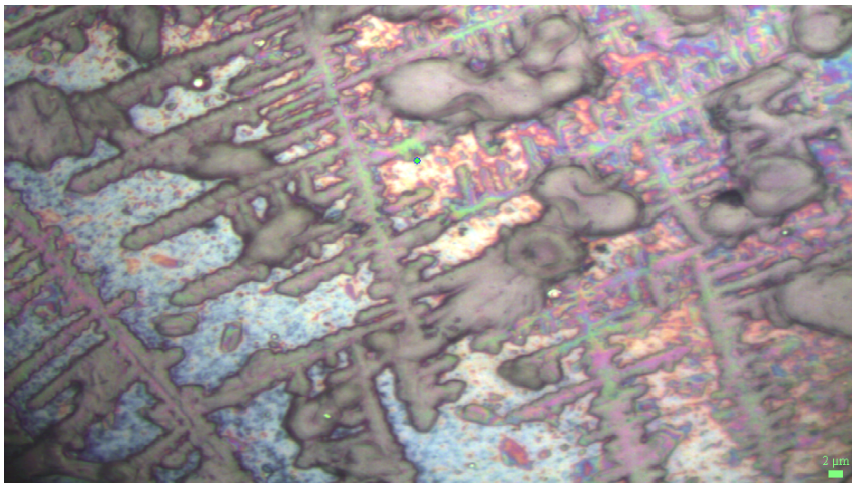

Figure 6.1: Surface of the SERS substarate surface after the deposition of the centrifuged solution.

Cleaning the saliva by centrifugation did not yield the desired results. Once the solution deposited on the SERS substrate evaporates, dendritic structures appear (Figure 6.1), this is likely due to crystallization of the salts present in the saliva. These dendritic structures cause a high fluorescence signal (Figure 6.3) which makes it unthinkable to use the spinnig cell setup.

6.1.2. Filtration through cotton swab

I prepared a solution of 1 ml of A diluted in saliva with concentration 10^{-4} M and pH=4. 100 μl of solution A was diluted in 900 μl of saliva and subsequently acidified with 10 μl of solution D.The solution was filtered through a cotton swab, about 1 cm thick, inserted into a Pasteur pipette. The prepared solution was poured into the Pasteur pipette and then mechanically forced through the filter. A droplet of the solution was deposited on a SERS substrate.

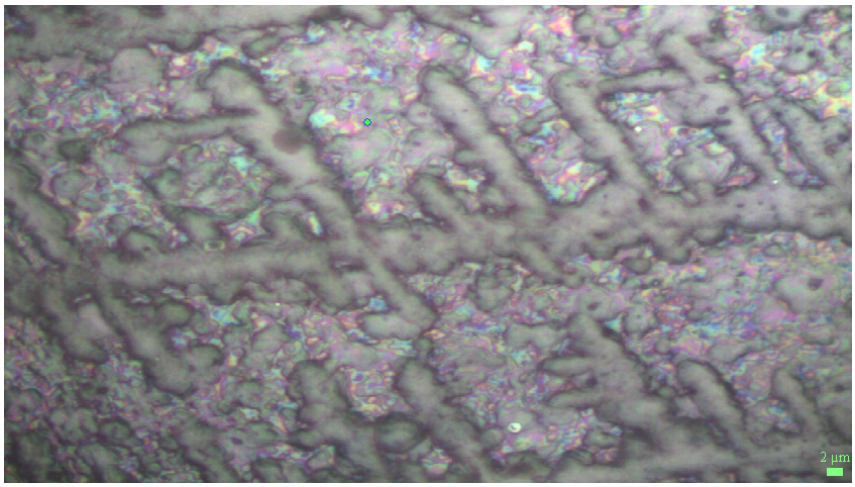

Figure 6.2: Surface of the SERS substrate surface after the deposition of the solution filtered through cotton swab.

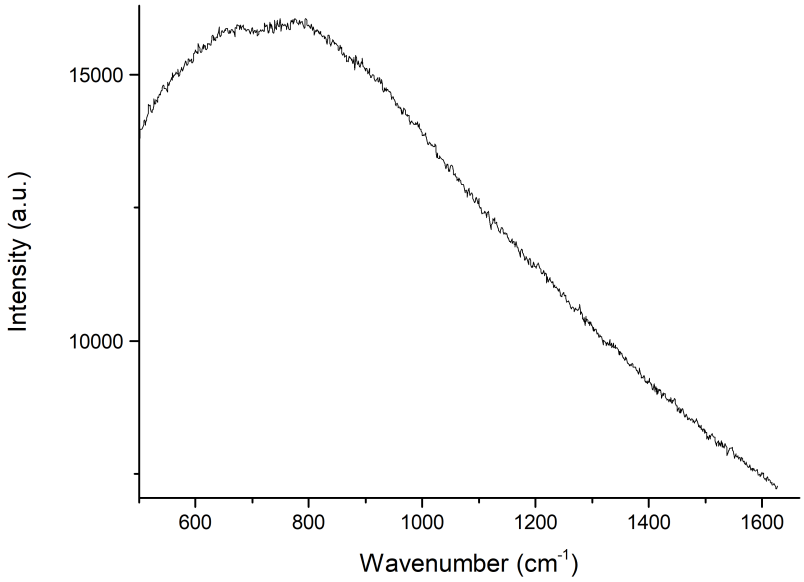

Figure 6.3: Example of a Raman spectrum biased by the fluorescence signal. Raman spectrum taken on a SERS pad n.19, using 633 nm laser excitation, 50x objective, 0.3 mW power, 120 seconds exposure time and 3 averages.

Filtering the saliva through a cotton ball did not yield the desired results. Once the solution deposited on the SERS substrate evaporates, dendritic structures appear (Figure 6.2), this is likely due to crystallization of the salts present in the saliva. These dendritic

structures cause a high fluorescence signal (Figure 6.3) which makes it unthinkable to use the spinnig cell setup.

6.1.3. Filtration through amorphous silica

The solution of PER diluted in saliva was prepared in the same way as shown in sections 6.1.2 and 6.1.1.

To filter the solution a 0.5 cm layer of amorphous silica (particle size 63/mum) was placed over a cotton ball inside a Pasteur pipette. The solution of PER diluted in saliva was poured into the pipette and forced mechanically through the silica filter. The filtered solution was collected in a test tube and a drop of it was deposited on a SERS substrate.

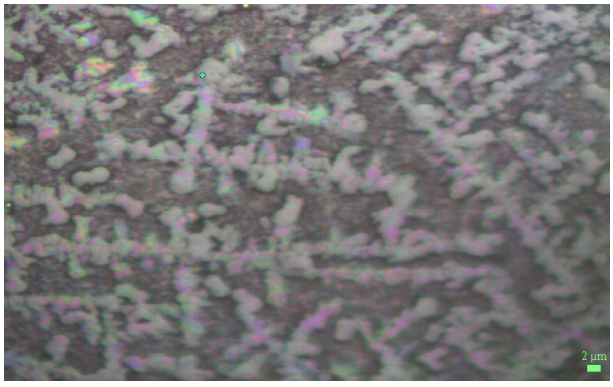

Figure 6.4: Image of the SERS substrate surface after the deposition of the solution.

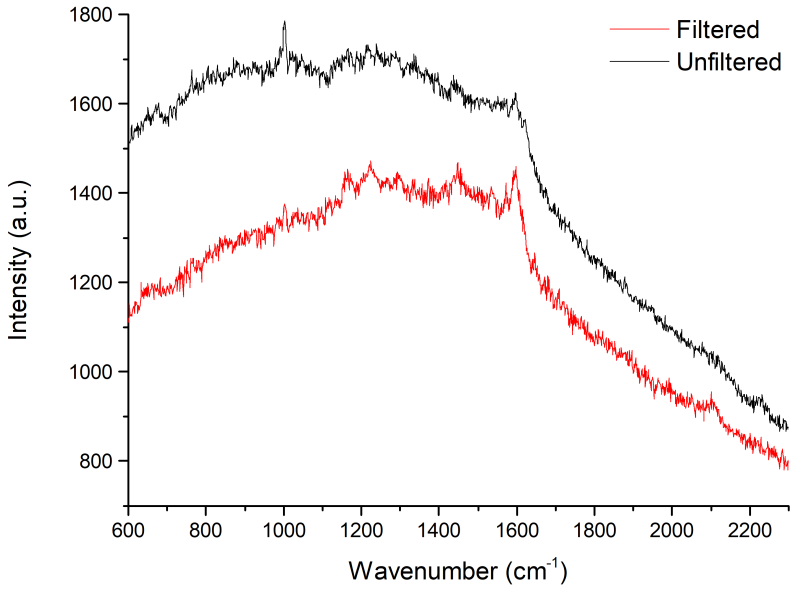

Figure 6.5: Confrontation of the Raman spectrum of the solution before and after the filtration. Collected on SERS substrate n.21, using 633 nm laser excitation, 50x objective, 0.3 mW power, 120 seconds exposure time and 3 averages.

The amorphous silica-filtered solution, once dried on the surface of the SERS substrate, also exhibits dendritic structures (Figure 6.4). These, however, do not appear to generate fluorescence in contrast to previous cases (see sections 6.1.1 and 6.1.2). From the SERS measurements it can be seen that the main markers of the PER are very weak (Figure 6.5), only the peaks at 1000 $cm^{-1}$and 1595 $cm^{-1}$are visible and in the case of the peak at 1000 cm^{-1}, this is much less intense than that measured on the unfiltered solution. One explanation for these results is that amorphous silica also retains PER during filtration. It is therefore necessary to do further analysis to ascertain whether the filtering action of the silica is too stringent and also excludes the PER.

To ascertain whether silica does indeed retain PER during filtration, UV-Vis spectroscopy measurements were made on solutions of PER diluted in distilled water.

Two solutions were prepared by diluting 90 μl of solution A with 2910 μl of distilled water to obtain a final solution with a PER concentration of 3×10^{-5} M. One of the two solutions was acidified with 4 μl of solution D so as to raise the pH of the solution to 4. Absorption spectra of the two solutions were obtained using the JASCO V-570 spectrophotometer.

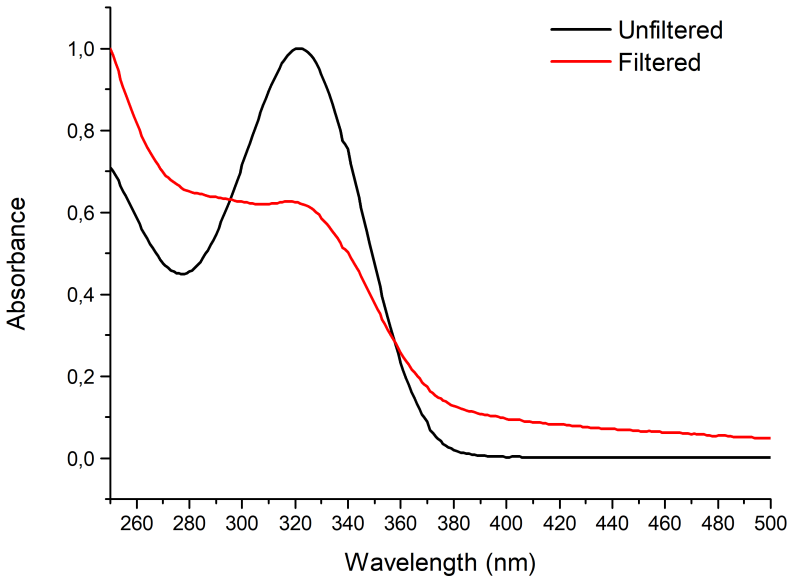

(a)

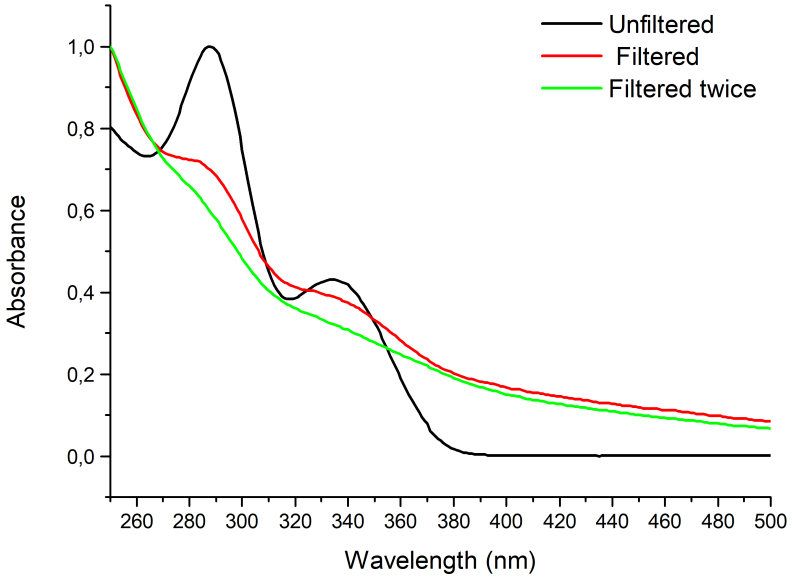

(b)

Figure 6.6: Normalized absorption spectra a) solution acidified before and after filtration, b) neutral solution before and after filtration.

By analyzing the UV-Vis spectra (Figure 6.6) it is possible to state the PER is retained by the amorphous silica filter. For both neutral and acidified solution, a drastic decrease

in the absorbance peaks typical of PER is observed. In the light of this evidence also the process of filtration by amorphous silica must be discarded from the shortlist of processes to be used to clean solutions of PER diluted in saliva.

6.1.4. Phase separation process

The phase separation technique is the latest process studied to clean up the solution of PER diluted in saliva. In this technique, the different solubility of PER in water and chloroform and the immiscibility of chloroform with aqueous solutions are exploited to bring PER dissolved in saliva from the phase in saliva to the phase in chloroform. A solution of PER dissolved in saliva was prepared and then chloroform was added in a 1:1 volume ratio with the PER/saliva solution. The solution was then stirred for 1 hour using a mechanical stirrer. Next, the solution was centrifuged at 5000 rpm for 20 minutes. After centrifugation, three phases can be distinguished (Figure 6.7), at the top the aqueous phase, in the middle a semi-solid phase consisting of the high molecular weight components of saliva and at the bottom the chloroform phase.

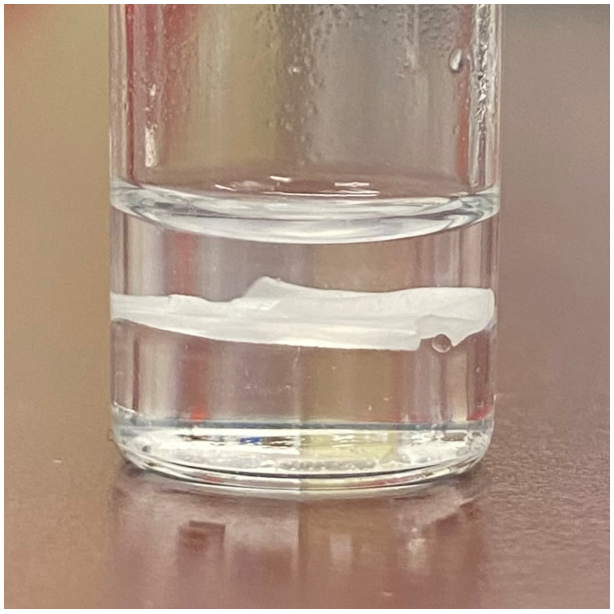

Figure 6.7: Image of the three phases after the centrifugation. At the top the water phase, in the middle the semi-solid phase and at the bottom the chloroform phase.

The chloroform phase was extracted and diluted with other pure chloroform in a volumetric ratio of 1:3 to obtain a clear solution in order to avoid light scattering phenomena during UV-Vis spectroscopy caused by turbidity of the solution. Finally, the solution was analyzed by UV-Vis spectroscopy. Here a list of all the steps of the process:

1. Preparation of the saliva/PER solution.
2. Add of chloroform in 1:1 volume ratio.
3. Stirring for 1 hour.
4. Centrifuge at 5000 rpm for 20 minutes.
5. Sampling of the chloroform phase.
6. Add in the solution sampled in step 5 of chloroform in 1:3 volume ratio.

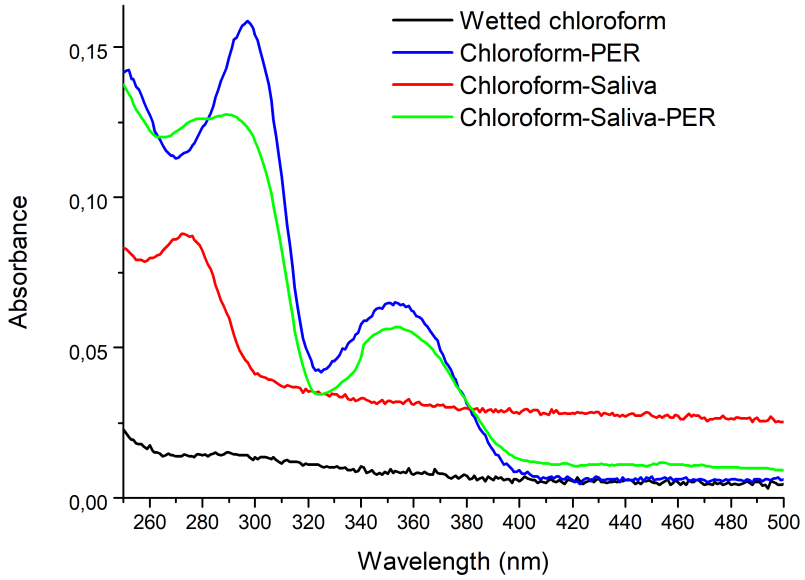

Figure 6.8: Absorption spectra of different solutions treated by the phase separation process.

The presence of the drug in the chloroform phase is confirmed by the absorbance peak at 350 nm (the green line in figure 6.8).

Five different solutions of PER and chloroform were prepared to plot a calibration curve for the purpose of calculating the molar extinction coefficient. The solutions were prepared using the process described above. The composition of the solutions and concentration after step 1 and step 6 are shown in table 6.1.

A	Saliva	PER conc. after step 1	PER conc. after step 6
80 μl	1920 μl	4×10^{-5}	10^{-5} M
64 μl	1936 μl	3.2×10^{-5}	8×10^{-6} M
48 μl	1942 μl	2.4×10^{-5}	6×10^{-6} M
40 μl	1960 μl	2×10^{-5}	5×10^{-6} M
16 μl	1984 μl	8×10^{-6}	2×10^{-6} M

Table 6.1: Recipes of the solutions prepared following the process decribed above that have been tested with UV-Vis spectroscopy.

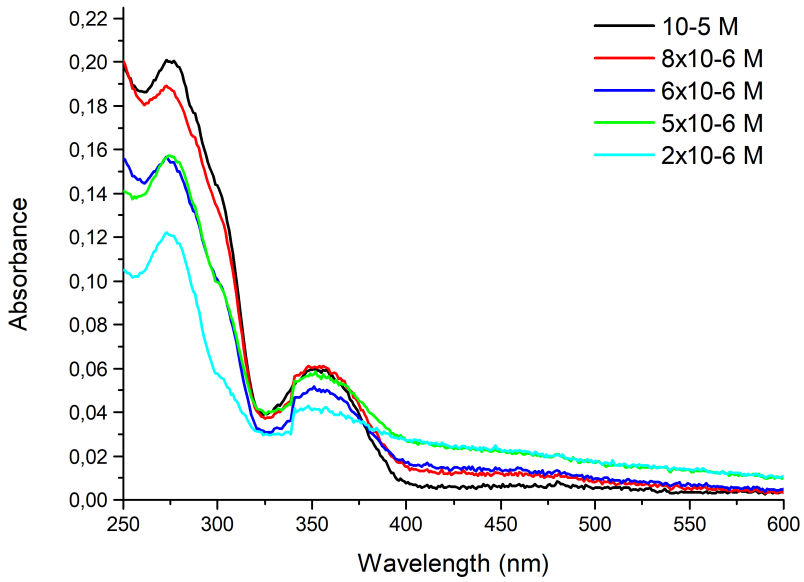

Figure 6.9: Absorption spectra of the different solutions reported in table 6.2.

PER concentration (M)	Absorbance at 350 nm
1×10^{-5}	0.053
8×10^{-6}	0.046
6×10^{-6}	0.034
5×10^{-6}	0.031
2×10^{-6}	0.014

Table 6.2: Baseline corrected value of absorbance of the solutions reported in table 6.1 at 350 nm.

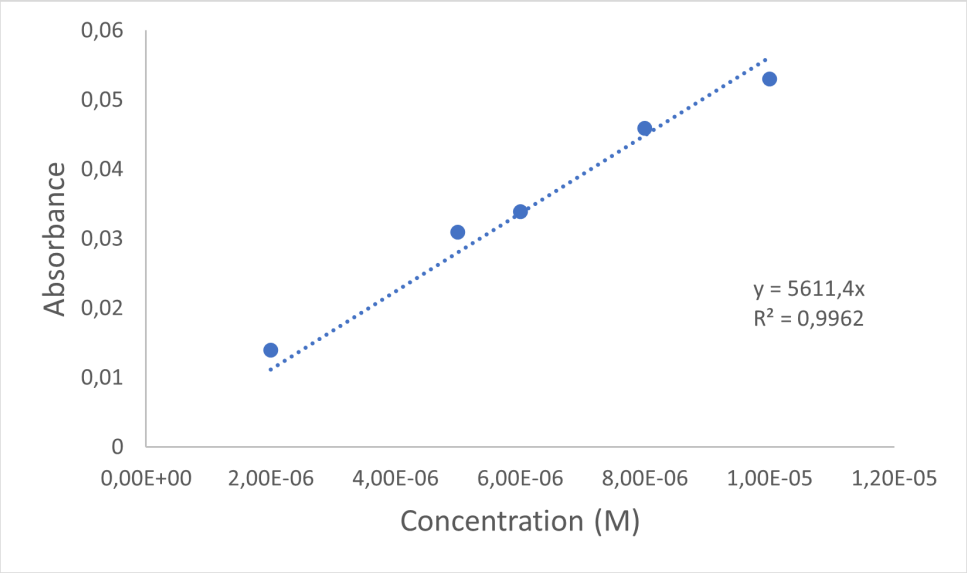

Figure 6.10: Calibration curve drawn using the data from table 6.2.

The peak at 350 nm was used to perform the molar extinction coefficient calculation. The height of the peak was measured for each concentration correlated with the height of the absorbance peak. The data were interpolated from a straight line passing through the origin (Figure 6.10). The interpolation coefficient is proportional to the molar extinction coefficient according to the Lambert-Beer law:

$$A = \varepsilon_\lambda C l \tag{6.1}$$

ε_λ is the molar extinction coefficient its dimensions in the I.S. are cm^2/mol. From the calculations it appears that since L=1 cm, ε_λ =5.61×10^6 cm^2/mol.

In order to evaluate the partition coefficient of PER between the aqueous phase and the chloroform phase, additional UV-Vis spectroscopy analysis was performed. For this purpose, the method of preparing the solutions was changed. The new process is as follows:

1. Sampling of Saliva.
2. Addition of chloroform in 1:1 volume ratio.
3. Stirring for 1 hour.
4. Centrifuge at 5000 rpm for 20 minutes.
5. Sampling of the chloroform phase.
6. Add in the solution sampled in step 4 of known volume of solution A.
7. Add in the solution sampled in step 6 of chloroform in 1:3 volume ratio.

Through this process it is possible to obtain solutions that has a known PER concentration. Thus, by comparing the absorption spectra of solutions with known concentration with those of solutions with uncertain concentration, it is possible to estimate the partition coefficient between the phase in saliva and the phase in chloroform.

Five different solutions were prepared to plot a calibration curve for the purpose of calculating the molar extinction coefficient. The solutions were prepared using the new process described above. The composition of the solutions and concentration after step 6 and 7 are given in the table 6.3.

Sol. A	Chloroform	PER conc. after step 6	PER conc. after step 7
20 μl	480 μl	4×10^{-5}	10^{-5} M
16 μl	484 μl	3.2×10^{-5}	8×10^{-6} M
12 μl	488 μl	2.4×10^{-5}	6×10^{-6} M
10 μl	490 μl	2×10^{-5}	5×10^{-6} M
4 μl	496 μl	8×10^{-6}	2×10^{-6} M

Table 6.3: Recipes of the solutions at well-known concentration tested with UV-Vis spectroscopy.

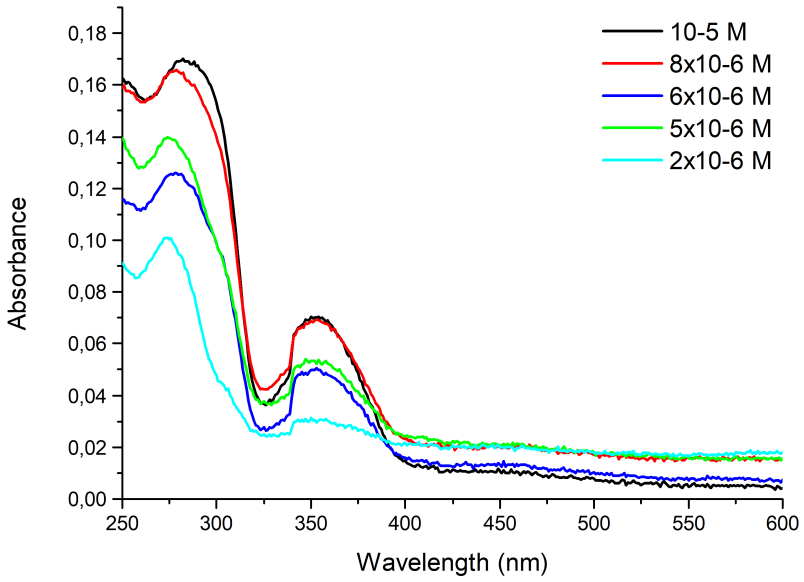

Figure 6.11: Absorption spectra of the different solutions reported in table 6.3.

PER concentration (M)	Absorbance at 350 nm
1×10^{-5}	0.056
8×10^{-6}	0.047
6×10^{-6}	0.032
5×10^{-6}	0.03
2×10^{-6}	0.0107

Table 6.4: Baseline corrected value of absorbance of the solutions reported in table 6.3 at 350 nm

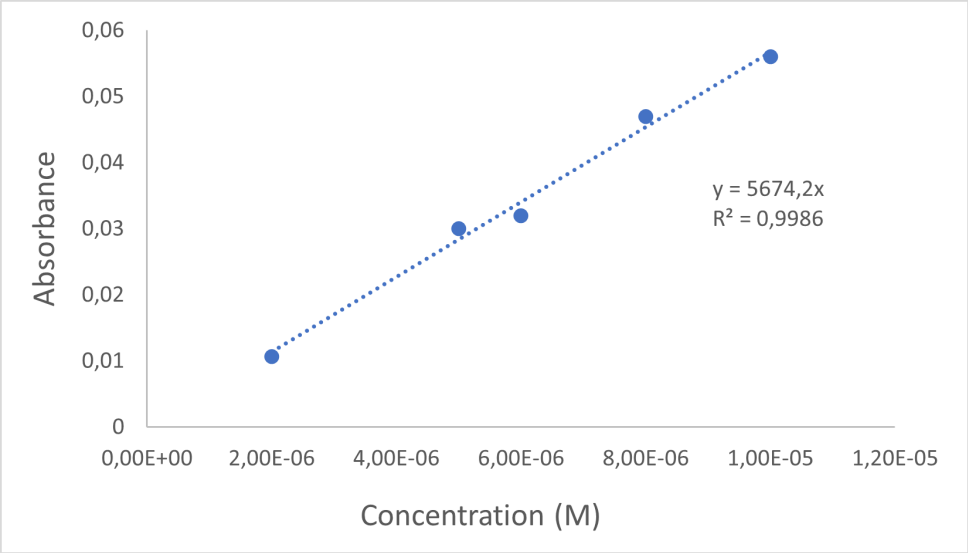

Figure 6.12: Calibration curve drawn using the data from table 6.4.

Comparing the absorbance values in the tables 6.2 and 6.4 we see that they are almost identical. It is therefore possible to say that the extraction of Perampanel from saliva by means of chloroform, in the limit of experimental error, has an efficiency of 100%.

This result allows us to consider the process of phase separation for the preparation of new samples to be analyzed by SERS spectroscopy.

6.2. Improvement of PER detection by SERS

Given the results obtained in section 6.1.4, a solution of PER diluted in saliva to a concentration of 5×10^{-4} M was prepared and then processed using the phase separation method shown in section 6.1.4. A drop of the extract was deposited on a SERS substrate.

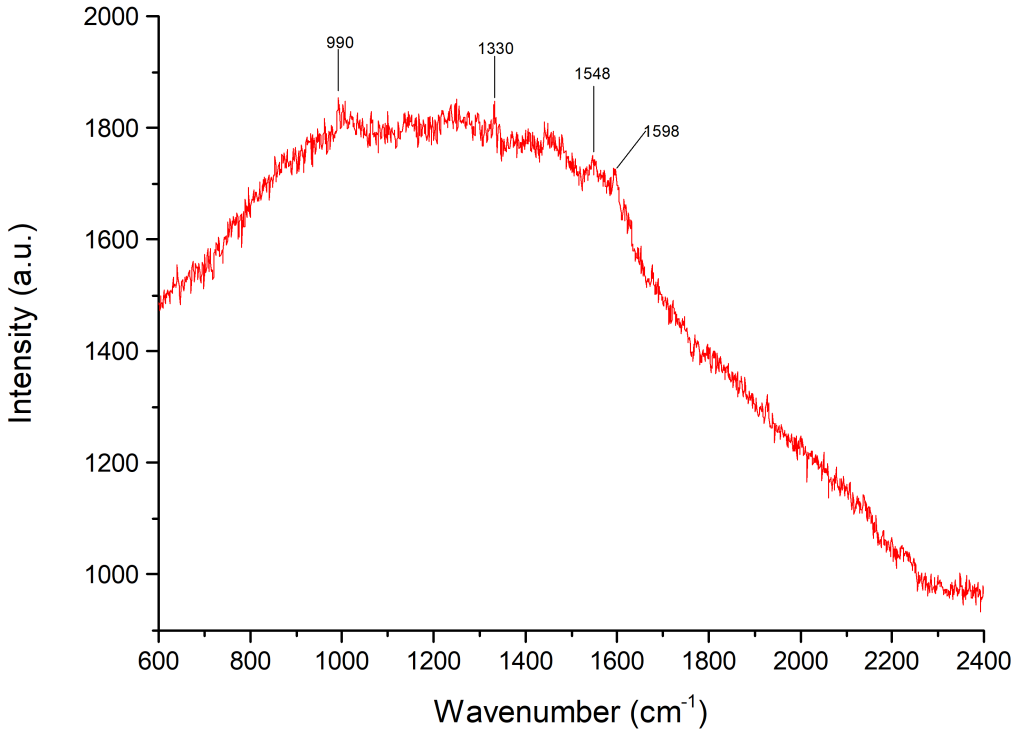

Figure 6.13: Raman spectrum of the PER-chloroform solution. Collected on SERS substrate n.25, using 633 nm laser excitation, 50x objective, 0.3 mW power, 120 seconds exposure time and 3 averages.

The chloroform phase turns out to be incompatible with SERS analysis. The typical peaks of PER are barely sketched (Figure 6.13) despite the high concentration of drug present in the solution. This result can be attributed to the inability to protonate the diluted PER in chloroform. The lack of protonation causes a weakening of the Raman response as verified in previous theses [27]. Two additional steps were added to the phase separation process to solve this problem. The chloroform extract is evaporated and the solid residue is solubilized using methanol. Finally, solution C is added which serves two functions: to acidify the PER and to provide the chlorine needed to bridge the nanoparticles on the SERS pad to the protonated PER.

A solution of PER diluted in saliva 5×10^{-4} M was prepared and treated as follows:

1. Preparation of 1 ml of PER diluted in saliva 5×10^{-4} M.
2. Add of chloroform in 1:1 volume ratio.

3. Stirring for 1 hour.
4. Centrifuge at 5000 rpm for 20 minutes.
5. Extraction of 300 μl of the chloroform phase.
6. Drying of the extracted solution.
7. Adding of 100 μl of methanol.
8. Adding of 200 μl of solution C.

The final solution was transferred to a vial from which a drop was taken and deposited on a SERS substrate.

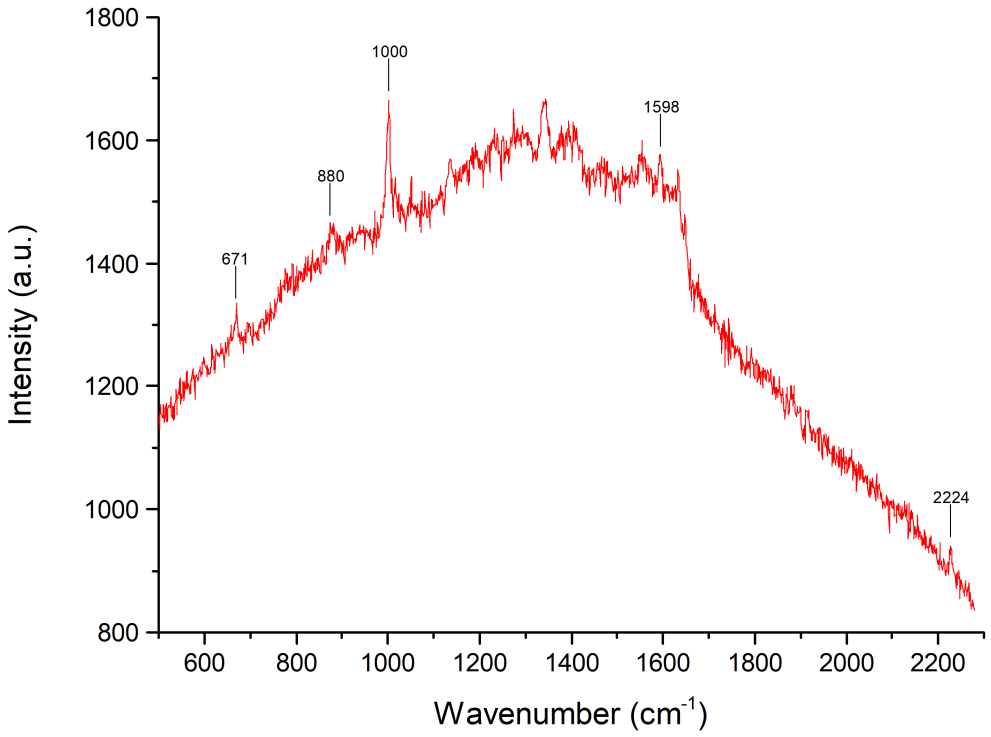

Figure 6.14: Raman spectrum of the solution fo PER acidified diluted in methanol. Collected on SERS substrate n.12, using 633 nm laser excitation, 50x objective, 0.3 mW power, 120 seconds exposure time and 3 averages.

All the PER markers are clearly visible in the spectrum obtained from the analysis of the solution obtained after phase separation and solubilization of the solid residue (Figure 6.14). This result allows to validate the process designed for the pre-treatment of saliva

samples. An interesting aspect of this process is the possibility, once the chloroform is evaporated (step 6), to obtain solutions of PER diluted in methanol that are more concentrated than the starting solution. For example, by pulling to dryness 1 ml of a solution of PER diluted in chloroform and solubilizing the dry residue with 10 mul of methanol it is possible to obtain a solution with a PER concentration greater by a factor of 10^2.

One such experiment was done to see if it was possible to detect at SERS analysis the PER from solutions having such a concentration of drug that it would not normally be detectable.

I prepared a solution of PER diluted in saliva to a concentration of 10^{-7} M by diluting 200 μl of a solution of PER 10^{-6} M diluted in methanol and distilled water with 1800 μl of saliva.

The solution was treated following the separation process that is reported here:

1. Preparation of 2 ml of PER diluted in saliva 10^{-7} M.
2. Add of 2 ml of chloroform.
3. Stirring for 1 hour.
4. Centrifuge at 5000 rpm for 20 minutes.
5. Extraction of 1 ml of the chloroform phase.
6. Drying of the extracted solution.
7. Adding of 50 μl of methanol.
8. Adding of 50 μl of solution C.

Given what was demonstrated in the 6.1.4 section, it can be assumed that all of the PER diluted in saliva passes into the chloroform phase so the concentration of PER in chloroform will be 10^{-7} M. Solubilizing the solid residue, obtained by evaporating 1 ml of PER solution in chloroform, with 100 total mul between methanol and C solution will result in a 10-fold more concentrated solution.

A drop of the solution was deposited on the surface of a SERS substrate for analysis.

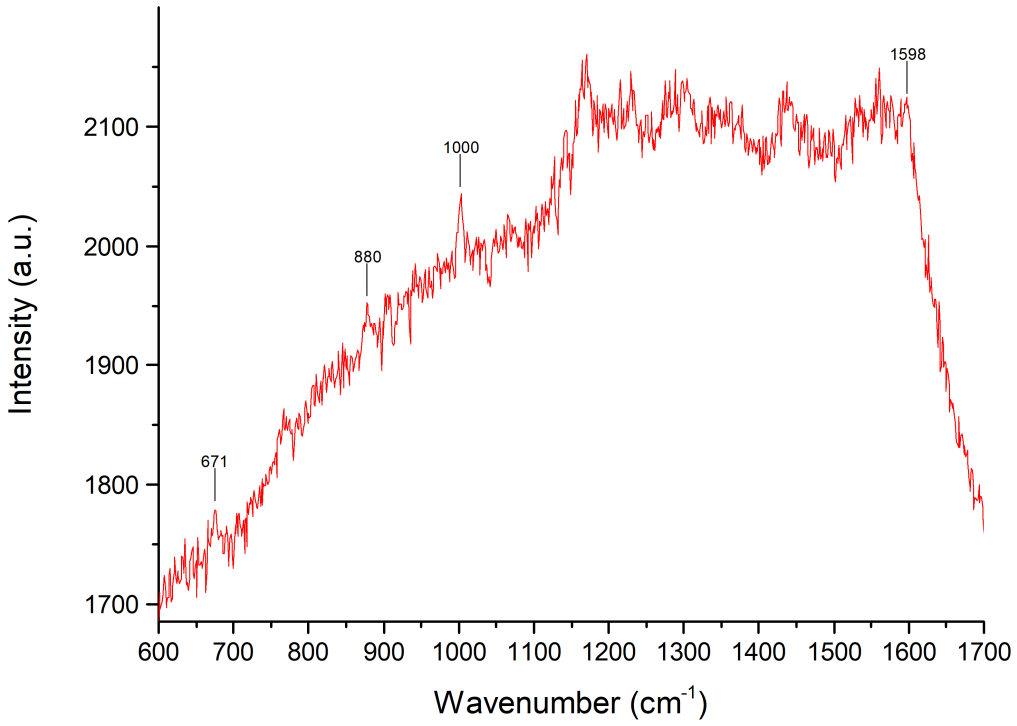

Figure 6.15: Raman spectrum of the solution of PER acidified diluted in methanol obtained using the phase separation methods. Collected on SERS substrate n.9, using 633 nm laser excitation, 50x objective, 0.3 mW power, 120 seconds exposure time and 3 averages.

In the SERS spectrum of the solution treated by the phase separation process, the PER markers are clearly visible (Figure 6.15). It is therefore possible, by appropriate pretreatment of the analyte, to detect PER present in saliva solutions at low concentrations. In this case we have concentrated the PER only by a factor of 10, but ideally it is possible to concentrate the PER by a much greater factor and in this way detect the drug even in saliva samples with lower concentrations. We can then approach the detection of PER diluted in saliva at concentrations around 10^{-9} M that is the concentration value of PER assumed to be present in the saliva of a real patient.

7 | Conclusions

In this thesis work, I was able to demonstrate the possibility of detecting dilute PER in saliva through SERS analysis. I was able to determine the qualitative response of SERS sensors to solutions with varying concentrations of PER. Finally, I developed a process to pre-treat the saliva samples in order to obtain solutions that allow for more accurate SERS measurements.

Raman measurements performed on my saliva have shown that the Raman response is constant and reproducible; this result allows for validation of the chosen sampling method. Furthermore, the analysis of the Raman spectra shows that the typical signal of saliva does not overlap with the main markers chosen for the PER (apart from the 1000 cm^{-1}marker).

It is shown that it is possible to detect dilute PER in saliva using SERS spectroscopy. Typical PER markers are visible with concentrations of PER as low as 5×10^{-6} M.

The signal intensity of the PER present in saliva in SERS analysis was shown to be linearly proportional to the concentration of the drug in solution. It was possible to draw calibration straight lines with respect to the PER markers. These straight lines have a reasonable degree of accuracy, with an R^2 between 0.66 and 0.91, depending on the marker considered.

The quantitative analysis was found to be disturbed by the presence of a high noise floor caused by the presence of a strong fluorescence signal. For this reason, a method of saliva treatment was considered so that more accurate measurements could be made. Treatment of saliva by a phase separation extraction process using chloroform proved to be an effective method for the purpose. Using UV-Vis analysis, it was shown that, within the limits of experimental error, it is possible to extract all of the diluted PER in saliva from the saliva phase to the chloroform phase. Finally, it was shown that by properly treating the PER extract solubilized in chloroform, it is possible to regain a solution of PER diluted in methanol that can be acidified. In the SERS signal of this solution the PER markers are clearly visible demonstrating that the whole phase separation process is a viable route to obtaining more accurate SERS measurements. Finally, it was shown that it is possible to obtain solutions with a good SERS response starting from solutions

containing a low concentration of PER (10^{-7} M).

Treatment of the solution by phase separation opens the door to the possibility of approaching PER detection in solutions with low concentrations (10^{-9} M). This is possible because, through evaporation of the diluted PER solution in chloroform, it is possible, to refocus the PER and in this way obtain methanol solutions with higher drug concentrations than those of the starting chloroform solutions. The methanol solutions can then be optimized for the range of the SERS PLD sensors.

Bibliography

[1] N. Agarwal, P. Ossi, and S. Trusso. Driving electromagnetic field enhancements in tailored gold surface nanostructures: Optical properties and macroscale simulations. *Applied Surface Science*, 2018.

[2] E. Cabassi and A. Marini. The saliva. complementary approach in clinical diagnostic and in biological research. In *Annali della Facolta'di Medicina Veterinaria-Universita'degli Studi di.* Parma (Italy, 2002.

[3] S. Chiappin, G. Antonelli, R. Gatti, and E. F. De Palo. Saliva specimen: a new laboratory tool for diagnostic and basic investigation. *Clin. Chim. Acta*, 383(1-2): 30–40, Aug. 2007.

[4] S. Crouch, D. Skoog, and F. Holler. *Principles of Instrumental Analysis.* CENGAGE Learning Custom Publishing, 7 edition, Jan. 2017.

[5] M. Danhof and D. D. Breimer. Therapeutic drug monitoring in saliva. *Clin. Pharmacokinet.*, 3(1):39–57, Jan. 1978.

[6] P. E. Eric Le Ru. *Principles of Surface-Enhanced Raman Spectroscopy.* Elsevier, 2009.

[7] S. Gittings, N. Turnbull, B. Henry, C. J. Roberts, and P. Gershkovich. Characterisation of human saliva as a platform for oral dissolution medium development. *Eur. J. Pharm. Biopharm.*, 91:16–24, Apr. 2015.

[8] L. Giuliani. Sers of perampanel for therapeutic drug monitoring using substrates produced by pld. Master's thesis, 2018.

[9] A. C. Gonçalves, F. A. L. Marson, R. M. H. Mendonça, C. S. Bertuzzo, I. A. Paschoal, J. D. Ribeiro, A. F. Ribeiro, and C. E. Levy. Chloride and sodium ion concentrations in saliva and sweat as a method to diagnose cystic fibrosis. *J. Pediatr. (Rio J.)*, 95 (4):443–450, July 2019.

[10] S. P. Humphrey and R. T. Williamson. A review of saliva: normal composition, flow, and function. *J. Prosthet. Dent.*, 85(2):162–169, Feb. 2001.

[11] J. S. Kang and M. H. Lee. Overview of therapeutic drug monitoring. *Korean J. Intern. Med.*, 24(1):1–10, Mar. 2009.

[12] E. Kaufman and I. B. Lamster. The diagnostic applications of saliva–a review. *Crit. Rev. Oral Biol. Med.*, 13(2):197–212, 2002.

[13] K. Kneipp, H. Kneipp, I. Itzkan, R. R. Dasari, and M. S. Feld. Surface-enhanced raman scattering and biophysics. *J. Phys. Condens. Matter*, 14(18):R597–R624, May 2002.

[14] M. D. Krasowski and G. A. McMillin. Advances in anti-epileptic drug testing. *Clin. Chim. Acta*, 436:224–236, Sept. 2014.

[15] D. A. Long. *The Raman Effect: A Unified Treatment of the Theory of Raman Scattering by Molecules*. Wiley, 2002.

[16] A. Macrelli. Development of paper-based sers sensors for the detection of drugs. Master's thesis, 2020.

[17] S. Maier. *Plasmonics: Fundamentals and Applications*. Springer, Dec. 2007.

[18] I. D. Mandel. The functions of saliva. *J. Dent. Res.*, 66 Spec No(2_suppl):623–627, Feb. 1987.

[19] A. Nurkka, J. Obiero, H. Käyhty, and J. A. G. Scott. Effects of sample collection and storage methods on antipneumococcal immunoglobulin a in saliva. *Clin. Vaccine Immunol.*, 10(3):357–361, May 2003.

[20] P. N. Patsalos and D. J. Berry. Therapeutic drug monitoring of antiepileptic drugs by use ofsaliva. *Ther. Drug Monit.*, 35(1):4–29, Feb. 2013.

[21] R. Pilot, R. Signorini, C. Durante, L. Orian, M. Bhamidipati, and L. Fabris. A review on surface-enhanced raman scattering. *Biosensors (Basel)*, 9(2):57, Apr. 2019.

[22] M. Pistaffa. Sers assessment of carbamazepine in methanol, chloroform and patient samples using au sensors with optimized surface nanostructrure. Master's thesis, 2017.

[23] P. Rekha, P. Aruna, B. Elumalai, D. Koteeswaran, M. Baludavid, and S. Ganesan. Near-infrared raman spectroscopic characterization of salivary metabolites in the discrimination of normal from oral premalignant and malignant conditions: Near-infrared raman spectroscopic characterization of salivary metabolites. *Journal of Raman Spectroscopy*, 47, 2016.

[24] J. Robertson, C. Hatton, E. Emerson, and S. Baines. Prevalence of epilepsy among people with intellectual disabilities: A systematic review. *Seizure*, 29:46–62, July 2015.

[25] A. Satlin, L. D. Kramer, and A. Laurenza. Development of perampanel in epilepsy. *Acta Neurol. Scand. Suppl.*, 127(197):3–8, 2013.

[26] E. Smith and G. Dent. *Modern Raman spectroscopy.* Wiley-Blackwell, 2 edition, Apr. 2019.

[27] N. S. Villa. Development of a sers technique for therapeutic drug monitoring: Case study on perampanel. Master's thesis, 2018.

[28] K. Virkler and I. K. Lednev. Forensic body fluid identification: the raman spectroscopic signature of saliva. *Analyst*, 135(3):512–517, Mar. 2010.

[29] T. Zelles, K. R. Purushotham, S. P. Macauley, G. E. Oxford, and M. G. Humphreys-Beher. Saliva and growth factors: the fountain of youth resides in us all. *J. Dent. Res.*, 74(12):1826–1832, Dec. 1995.